AN EXPERIMENTAL INVESTIGATION AND MODELLING INTO THERMAL CONDUCTIVITY OF NANOFLUIDS

A

THESIS

Submitted in partial fulfillment of the requirement for the award of degree of

Master of Engineering

In
Thermal Engineering

Submitted by

AMIT KUMAR

(ROLL NO: 801183001)

UNDER THE GUIDANCE OF

Dr. S.S. MALLICK

(ASSISTANT PROFESSOR)

Department of Mechanical Engineering

Thapar University, Patiala

July, 2013

CERTIFICATION

I, Amit Kumar, declare that this thesis report, submitted toward fulfillment of the requirements for the award of Master's degree in Thermal engineering in the Mechanical Department, Thapar University, Patiala, is wholly my own work. This document has not been submitted for any degree at any other institution.

Date: 12/7/13
Place: PATIALA.

Amit Kumar
801183001
Thapar University, Patiala

This is to certify that the above statement made by the candidate is correct and true to the best of my knowledge.

12/7

Guide:
Dr. S.S. Mallick
Assistant Professor
Mechanical Engineering Department
Thapar University, Patiala

Countersigned by

Dr. Ajay Batish
Professor and Head
Mechanical Engineering Department
Thapar university, Patiala

Dr. S.K. Mohapatra
Senior Professor and
Dean of Academic Affairs
Thapar university, Patiala

ii

ACKNOWLEDGEMENT

No volume of words is enough to express my gratitude towards my guide**,** Dr. S.S. Mallick, Department of Mechanical Enineering, Thapar University, Patiala, who has been very concerned and has aided for all the material essential for the preparation of this report. He has helped me explore this vast topic in an organized manner and provided me with all the ideas on how to work towards a research-oriented venture.

I would also like to thank, Dr. Bonamali Pal, School of Chemistry and Biochemistry, Thapar University, Patiala, and Mr. Bhupinder Pal, research scholar, School of Chemistry and Biochemistry, Thapar University, Patiala, who were always there at the need of the hour and provided with all the help and facilities, which I required, for the completion of my report work.
I would also thank to Thapar University, Patiala for providing funds to my thesis work.

Most importantly, I would like to thank my parents and the almighty for showing me the right direction out of the blue, to help me stay calm in the oddest of the times and keep moving even at times when there was no hope.

Amit Kumar
801183001
Thapar University, Patiala.

CONTENT **PAGE NO.**

ABSTRACT

In this study, the thermal conductivity of manufactured ZnO-water, ZnO-ethylene glycol, single wall carbon nanotubes (SWCNT)-water and silver aqueous solution nanofluids have been evaluated. The effect of sonication time, settling time, temperature, particle size and volume fraction have been studied on the thermal conductivity of manufactured nanofluids. The results shows as the sonication time increases (0-8 hours), the maximum enhancement in the thermal conductivity of ZnO-water and ZnO-ethylene glycol nanofluids are 11.3% and 3.5% respectively of volume fraction 0.05% at a temperature 25° C. The thermal conductivity of nanofluids decreases as the settling time rises. The effect of sonication power (140-220 W) of volume fraction 1% has been studied on the thermal conductivity of SWCNT nanofluid which, shows 2-11.5% increment at a temperature 25° C. A model has been proposed to calculate the thermal conductivity of nanofluids and the results of proposed model show reasonably good agreement with available experimental data.

Chapter 1: Introduction and Objectives

1.1 Introduction

The mixture of small solid particles (average size less than 100 nm) in to the basefluid (e.g ethylene glycol and DI water) is called nanofluid (Das et al. 2008). Dispersion of uniformly small amount (1 to 3% volume fraction) of nanoparticles in basefluid can improve the thermal conductivity of overall mixture (Das et al. 2008). As the thermal conductivity of solid particles is higher than those of basefluids, the heat transfer rate is expected to higher. Nanofluid can be used for cooling purposes in microchips, nuclear reactor, heat exchanger, radiator and transportation industry. e.g, the electronics industry could design computers with faster speed, high capacity, smaller size and expanded features. Air cooling is the best method for the electronic systems. However, heat fluxes over 100 W/cm^2 in electronic devices and system necessitate the use of liquid cooling. For enhancing heat transfer, earlier days coarse solid particle (μm or even mm sized) suspended in to the basefluid, which gave clogging and abrasion problems in small passages due to higher size (Chopkar et al. 2008 and Kwak et al. 2005).

In spite of the above potential uses (electronic and thermal application) of nanofluid in heat transfer application, still it is limited to be used commercially because it is difficult to develop models for thermal conductivity of nanofluids. It is difficult to understand the thermo physical behavior of nanofluid, as the mechanism of heat transfer contains many parameters (for nanofluids), such as the particle size/distribution, volume fraction, aspect ratio, use of surfactant, temperature, pH value of nanofluid, frequency, settling time and ultrasonication time.

There are number of theoretical models (Murshed et al. 2008; Yu and Choi, 2003 and Xie et al. 2005) and empirical models (Peterson et al. 2006 and Mintsa et al. 2009), for thermal conductivity of nanofluid, but all models have not been evaluated for wide range of nanofluids, so there is further need to evaluate and improve the existing models. Also, there is a need to

systematically investigate the effect of different particle and basefluid parameters (particle size/distribution, volume fraction, aspect ratio, use of surfactant, temperature, pH value of nanofluid, frequency, settling time and ultrasonication time) on the thermal conductivity of nanofluids. Previous reported research work (Murshed et al. 2008; Yu and Choi, 2003; Peterson et al. 2006 and Mintsa et al. 2009) have evaluated only few parameters in isolation such as particle size and volume fraction and reported literature generally do not mention all the experimental conditions. These researchers not studied the effect of sonication and settling time which is also parameters to study the effect on thermal conductivity of nanofluids. Hence, it is difficult to pin point the influence of a single parameter on thermal conductivity of nanofluids. In this experimental investigation ZnO, single wall carbon nanotubes and silver colloidal solution is being selected for the measurement of thermal conductivity of nanofluids because there has not been so much of investigation done on these nanofluids and study the thermal conductivity behaviour of nanofluids against sonication time, settling time and temperature. These parameters have been selected to measure thermal conductivity and to visualize the behaviour of nanoparticles in basefluids that whether cluster formation takes place or not.

1.2 Objectives

The specific objectives are:

1) To investigate the thermal conductivity of nanofluids with different nanoparticles such as ZnO, single wall carbon nanotubes and silver colloidal solution.
2) To evaluate the accuracy of existing models over the wide range of experimental data
3) Investigating the effect of sonication time, settling time and temperature on the thermal conductivity of nanofluids.
4) Development of model for thermal conductivity and validate against experimental data.

Chapter 2: Literature Review

2.1 Different Types of nanoparticles, basefluids and synthesis methods

Nanoparticles used in nanofluids are made of various materials, such as oxide ceramics (Al_2O_3 and CuO), nitride ceramics (AlN and SiN), carbide ceramics (SiC and TiC), metals (Cu, Ag and Au), semiconductors (TiO_2 and SiC) and carbon nanotubes. There are many types of basefluids such as water, ethylene glycol and oil (Das et al. 2008). Manufacturing of nanofluids can be classified into two categories: physical method and chemical method (Kimoto et al. 1963; Gleiter, 1989 and Granqvist and Buhrman, 1976). The basic principle for the synthesis of nanoparticles is to produce a large number of nuclei and to inhibit the growth and aggregation of grains (Ashly 1994). The physical method to obtain nanoparticles is normally carried out by millimg as is known for several metal nanoparticles. However, there are problems of oxide formation and contamination from the metal/ceramic balls. Among chemical methods, several low temperature techniques like precursor, co precipitation and solovothermal method used to avoid agglomeration and grain growth to produce nanoparticles.

2.1.1 Physical method:

High energy ball milling:

Top down approaches include milling or attrition and repeated quenching. Attrition can produce nanoparticles ranging from a couple of tens to several hundreds of nanometers in diameter. However, nanoparticles produced by attrition have a relatively broad size distribution and varied particle shape and geometry. In addition they may contain significant amount of impurities from milling medium defects resulting from milling. Such prepared nanostructures are commonly used in fabrication of nanocomposites. Repeated thermal cycling may also break a bulk material into small pieces, if the materials have very small thermal conductivity but a large volume changes as a function of temperature. A big volume change associated with phase transition can be

effectively utilized in this approach. Although very fine particles can be produced, this process is difficult to design and control so as to produce desired particle size and shape (Shah et al. 2010).

Arc discharge method:

A common technique for the production of single walled carbon nanotubes (SWNTs) is the electric arc discharge method in which carbon is vaporized between two carbon electrodes. Small diameter, single-wall nanotubes can be synthesized using a dc arc welder to maintain the optimal settings between two horizontal electrodes in helium or argon atmospheres. The voltage is controlled by an automatic feedback loop that senses the voltage differences between the two electrodes and adjusts them accordingly. The feedback system contains a motor and arc welder. The desired voltage must be set on the control box which signals the motor to separate or the electrodes to increases the voltage or bring the electrodes close together to decreases the voltage. This technique involves the generation of an electric arc between two graphite electrodes one of them is usually filled with catalyst metal powder in a helium atmosphere (Shah et al. 2010).

Laser ablation:

In laser ablation, high power laser pulses are used to evaporate matter from a target surface such that stoichiometry of the material is preserved in the interaction. As a result, a supersonic jet of particles (plume) is ejected normal to the target surface. The plume, similar to the rocket exhaust, expands away from the target with a strong forward directed velocity distribution of the different particles. The ablated species condense on the substrate placed takes place in a vacuum chamber either in vacuum or in the presence of some background gas. In the case of oxide films, oxygen is the most common background gas. In addition, the substrate temperature has to be sufficiently large (700-800°C) and uniform across the whole substrate area to obtain epitaxial films. This technique was observed in 1985 at the Rice University by Smally Group. Iron, gold, palladium

and compounds of sulphides have been prepared by this method. This method is capable of high rate of production of 2-3 g/min (Shah et al. 2010).

Aerosol synthesis:

In this method, a liquid precursor is first prepared. The precursor can be a simple mixture solution of desired constituent elements or a colloidal dispersion. Such a liquid precursor is than mystified to make a liquid aerosol i.e a dispersion of uniform droplets of liquids in a gas which may simply solidify through evaporation of solvent or further react with chemicals that are present in the gas. The resulting particles are spherical and their size is determined by the size of initial droplets and concentration of solid. Aerosol can be relatively easily produce by sonication or spinning (Shah et al. 2010).

Inert gas condensation:

Gas condensation was the first technique used to synthesis nanocrystalline metals and alloys. In this technique, a metallic or inorganic material is vaporized using thermal evaporation sources such as a joule heated refractory crucibles, electron beam evaporation devices, in an atmosphere of 1-50 mbar. In gas evaporation, a high residual gas pressure causes the formation of ultra fine particles (100 nm) by gas phase colloision. Vaporization sources may be resistive heating, high energy electron beams, low energy electron beam and including heating. Clusters form in the vicinity of the source by homogenous nucleation in the gas phase grew by incorporation by atoms in the gas phase. During heating, atoms condense in the supersaturation zone close to joule heating device. The nanoparticles are removed by scrapper in the form of a metallic plate. Evaporation is to be done from tungsten or molybdenum refractory metal crucibles. If the metals react with crucibles, electron beam evaporation technique is to be used. This method is extremely

slow. The method suffers from limitations such as a source-precursor incompatibility, temperature ranges and dissimilar evaporation rates in the alloy (Shah et al. 2010).

Chemical vapor deposition (CVD):

CVD is the process of chemically reacting a volatile compound of a material to be deposited, with other gases, to produce a non volatile solid that deposits atomistically on a suitably placed substrate**.** This well known process, in which a solid is deposited on a heated surface via a chemical reaction from the vapor or gas phase requires activation energy to proceed. This energy can be provided by several methods. In thermal, CVD the reaction is activated by a high temperature above 900°C. In plasma CVD, the reaction is activated by plasma at temperatures between 300 and 700°C. In laser CVD, pyrolysis occurs when laser thermal energy heats an absorbing substrate. In photo-laser CVD, the chemical reaction is induced by ultra violet radiation which has sufficient photon energy, to break the chemical bond in the reactant molecules (Shah et al. 2010).

2.1.2 Chemical method:

In crystal growth, growth species, such as atoms, ions and molecules, after impinging on the growth surface assemble into crystal structure one after another. This approach refers to the building-up of material from the bottom: atom by atom, molecule by molecule or cluster by cluster. Although the bottom up approach is nothing new it plays an important role in the fabrication and processing of nanostructures and nanomaterials. Nanomaterials of various oxides can be also be synthesized by confining chemical reaction, nucleation and growth process in small spaces such as micelle approaches. Various synthesized methods can be group into two categories: thermodynamic equilibrium approach or kinetic approach. In the thermodynamic approach, synthesis process consists of (a) generation of supersaturation (b) nucleation and (c)

subsequent growth. Following are the chemical methods to synthesized nanoparticles: (Shah et al. 2010).

Solovothermal synthesis:

A solvent is mixed with certain metal precursors and the solution mixture is placed in an autoclave kept at relatively high temperature and pressure in an oven to carry out the crystal growth and assembly process. The pressure generated in the vessel due to the solvent vapor elevates the boiling point of the solvent. Typically solovothermal methods make use of solvent such ethanol, methanol and toluene. This has been employed to synthesis oxides with and without the aid of surfactants. In this method, nanophase materials are produced by chemical reactions in an aqueous or organic medium under the simultaneous application of heat and pressure in the presence of an alkali or acid (Shah et al. 2010).

Hydrothermal synthesis:

Hydrothermal synthesis can be defined as a method of synthesis of single crystals which depends on the solubility of minerals in hot water under high pressure. The crystal growth is performed in an apparatus consisting of a steel pressure vessel called autoclave, in which a nutrient is supplied along with water. A gradient of temperature is maintained at the opposite ends of the growth chamber so that the hotter end dissolves the nutrient and the cooler end causes seeds to take additional growth (Shah et al. 2010).

Co-precipitation:

The co precipitation technique is a useful method for the preparation of ceramic oxide powders. In the this method, the required amount of the aqueous solution of desired metal ions gets precipitated by adding solution of ammonia, ammonium hydroxide or ammonium carbonate. The

precipitate was washed with distilled water, dried and ground to obtain particles of sizes smaller than 5 μm (Shah et al. 2010).

2.2 Measurement technique of thermal conductivity for nanofluids

There are mainly two methods for measurement of thermal conductivity steady state method and transient methods (Das et al. 2008). Transient hot wire method and temperature oscillation are the two transient methods. Steady state methods are less accurate than transient methods because in steady state methods heat lose cannot be quantified and may provide considerable inaccuracy and natural convection may also set in, which provides apparently higher value of thermal conductivity (Das et al. 2007).

2.2.1 Transient hot-wire method

In transient hot wire method, a thin metallic (platinum, KD2 pro instrument) needle is used as both a line heat source and temperature sensor. The needle is surrounded by the liquid whose thermal conductivity is to be measured. The diameter of needle is 1.3 mm and 60 mm long and having thermal conductivity range 0.02 to 2.0 W/mK. A single reading generally takes 2 minutes. The first 90 seconds are used to ensure temperature stability, after which the KD2 probe is heated for 30 seconds using a known amount of current. The reading is noted in data acquisition system which is connected to KD2 probe. The experimental setup shown schematically in Figure 2.1.

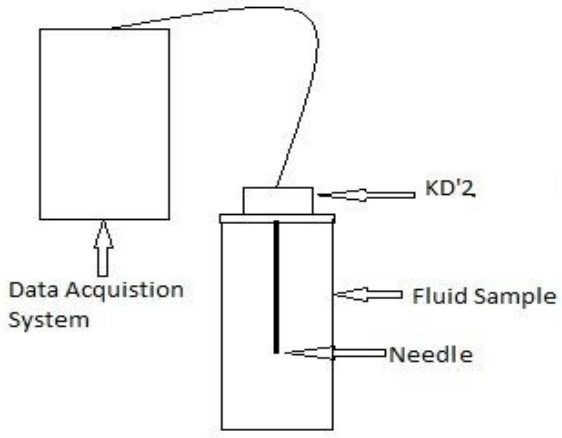

Figure 2.1: Schematic of experimental setup

Murshed et al. (2005) explained the apparatus specifications of transient hot wire method, the diameter of platinum wire 76 μm, length 215 mm, volume of container is 80 ml and diameter of container is 20 mm. The main experimental cell is a part of wheatstone bridge circuit, in which platinum wire is used as an arm of the wheatstone bridge circuit, which have high electrical resistivity and order of higher magnitude than that of any other material and the temperature coefficient resistance of platinum wire has 0.0039092 °C (Das et al. 2007; Murshed et al. 2005). The Wheatstone bridge circuit was balanced by adjusting the adjustable circuit resistance and ground resistance of A/D (analog to digital) converter input panel. Circuit was considered as balance circuit when there no voltage change observed in A/D converter. When a uniform voltage is supplied to the circuit, the temperature and electric resistance of the wire rises and the output voltage is measured by an A/D convertor. The obtained data of temperature rise is linear against logarithmic time interval. The thermal conductivity is calculated from the slope of the rise in the wire's temperature against logarithmic time interval by the equation 2.1(Das et al. 2007).

$$K_{n_f} = \frac{Q}{4\pi(T_2 - T_1)} \ln \frac{t_2}{t_1} \qquad (2.1)$$

2.2.2 Transient short hot wire method (SHW)

Zhang et al. (2000) used transient short wire method to measure the thermal conductivity and thermal diffusivity of nanofluids. This technique is based on the two-dimensional transient heat conduction numerical solution for a short wire of the same length-to-diameter ratio and boundary conditions as those used in the actual measurements. The thermal conductivity of nanofluids in transient SHW technique is calculated by equation 2.2 (Zhang et al. 2000):

$$K_{n_f} = \frac{VI}{\pi h} \cdot \frac{E}{e} \tag{2.2}$$

'E' calculated from the least squares method for a relevant range of Fourier number corresponding to the periods of measurement and 'e' calculated from the least squares method for time range before the onset of natural convection.

The length of short platinum wire of 9.2 mm and diameter of 97 μm welded at the both ends to 1.5 mm diameter platinum lead wire which is supported by a ceramic circular plate and joined with voltage and current platinum lead wires of 0.5 mm diameter. A pure gold crucible is heated with an electric furnace which is thermal insulator from outside. Thermocouples mounted at the outside wall of crucible to measure temperature and give signal to the controller. At constant liquid temperature, a current of 15 mA supplied to the probe for 3 sec. The switch is closed to the main circuit to begin heating the hot wire, when the current becomes stable.

In temperature oscillation method, the mainly principle of measurement of thermal conductivity is based on the propagation of a temperature oscillation inside a cylindrical liquid volume. This technique requires a fabricated cell, which is cooled by cooling water, on both ends coming from a thermostatic bath. An electrical connection provides DC power obtained through a converter

peltier element. The temperatures are measured in the test section through thermocouples, and the responses are amplified using an amplifier followed by filter. The frame consists of main part with a 40 mm hole that acts cavity to hold the test fluid and two end plates. The hole in the main frame is closed from both sides with disk reference material 40 mm in diameter and 15 mm thick. Temperatures are measured at three locations at interface of the peltier element and the reference layer at the interface of the reference layer and the test fluid and at the central axis plane of the test fluid (Das et al. 2008).

2.2.3 Steady-state parallel-plate method

Principle of measurement: This method is used to measure the thermal conductivity of nanofluids, this method requires very small amount of liquid sample. Wang et al. (1999) used this method to measure the thermal conductivity of Al_2O_3 and CuO nanofluids. Figure 2.2 shows the experimental setup, which follows the design by Challoner and Powell, 1956. Fluid sample is placed between two parallel round copper plates. The surface of the fluid sample is slightly higher than the lower surface of upper plate. Any gas bubbles are avoided when fluid sample is filled into the cell. The cross-sectional area of the upper plate is 9.552 cm^2. Both the copper plates are separated by three small glass spacers. Each glass spacer is of 0.9652 mm in thickness and a total surface area of 13.76 mm^2. Liquid cell is housed in a larger aluminum cell to control the temperature of liquid cell. The top copper plate is centered and away from the inside wall of the aluminum cell. There is a hole of 0.89 mm diameter is drilled in aluminum cell and copper plates. Temperature is measured by inserting E-type thermocouples (nickel–chromium/copper–nickel) into these holes. Because the thermal conductivity of copper is much higher than the thermal conductivity of the liquid, thermocouples provide temperatures at the surfaces of the plates. Total 14 thermocouples are used. At the time of experiment heater 1 gives the heat flux

from upper plate to lower plate. Uniformity in temperature of the lower copper plate is maintained by heater 4. Heaters 2 and 3 are used to increase the temperature of the aluminum cell to that of the upper plate to eliminate radiation and convection losses from the upper copper plate. The temperature difference between the inside wall of the aluminum cell and upper copper plate is less than 0.05 $^{\circ}$C, during all measurements. The uniformity of temperature in the top and the bottom plates is better than 0.02 $^{\circ}$C. The difference of temperature between the two copper plates varies from 1 to 3 $^{\circ}$C. All the heat supplied by heater 1 is flows between both the copper plates. The overall thermal conductivity across the two copper plates, adding the effect of the three glass spacers, can be calculated by the one-dimensional heat conduction equation 2.3:

$$K = (P.X_g)/(a_c \Delta T) \tag{2.3}$$

Where, X_g=0.9652 mm, a_c=9.552 mm^2

Thermal conductivity of nanofluids is calculated by equation 2.4:

$$K_{nf} = \frac{K.a_c - K_g.a_g}{a - a_g} \tag{2.4}$$

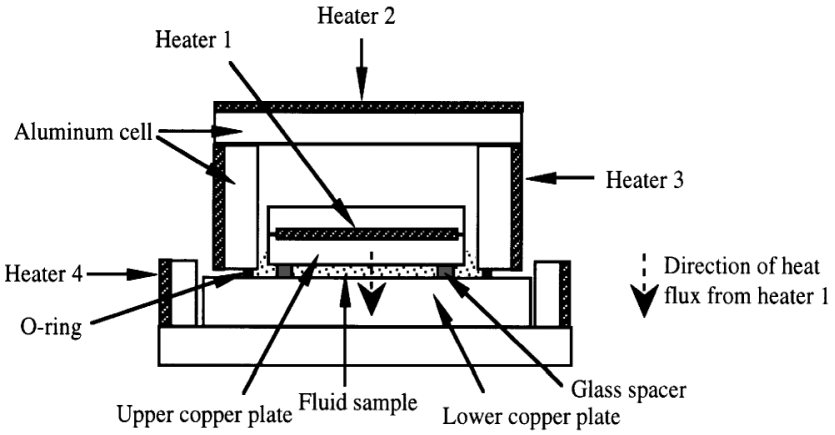

Figure 2.2: Schematic of experimental set up by Wang et al., 1999.

2.2.4 Steady state method

Principle of measurement: This steady state method which is referred as cut-bar apparatus had used for measuring the thermal conductivity of porous media and other materials (Li and Peterson, 2006). This method could be modified and extended to measure the thermal conductivity of nanofluids. Li and Peterson (2006) used this method to measure the thermal conductivity of Al_2O_3 based nanofluds. Figure 2.3, shows the schematic of apparatus. A pair of copper rods of 2.54 cm diameter is separated by O-ring to form a test cell setup. Several thermocouples are located in copper bars to measure the surface temperature and heat flux. Experimental test set up has to place in a vacuum chamber to perform experiments. Vacuum environment should be less than 0.15 Torr. By measuring the temperature differences in the copper bars, the heat flux in a traditional cut-bar apparatus can be determined. Using the heat flux obtains from equation 2.5 and surface temperature calculate by averaging the temperature obtained from thermocouples, the thermal conductivity of nanofluids can be calculated by equation 2.6:

$$Q = K_{copper} A_{bar} \frac{\Delta T_{bar}}{\Delta Z_{bar}} \tag{2.5}$$

$$K_{nf} = [Q(\Delta Z c_{ell} / \Delta T_{cell}) - K_{oring} A_{oring}] / A_{cell} \tag{2.6}$$

The test facility was calibrated to initiating the experimental test program. The two copper bars were aligned vertically and to ensure good contact, a load was applied using a load screw. The sample was charged through the lower sample charge inlet until the suspension filled the test cell setup and exited the charge outlet shown in Figure 2.3.

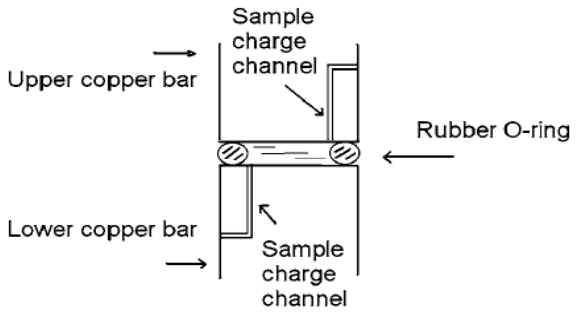

Figure 2.3: Schematic of experimental setup by Li and Peterson, 2006.

KD2Pro is a commercially available instrument to measure thermal conductivity of nanofluids. It uses the transient line heat source method to measure thermal conductivity.

2.3 Nanoparticle characterization and its importance

Characterization after synthesis of nanoparticles is very important because it gives the properties of synthesis materials, crystal structure of unknown materials, strain, crystal size, orientation of single crystal, grain size and particle size distribution in basefluid. Characterization of nanoparticles is done by the following methods:

Dynamic Light Scattering (DLS): DLS is used to characterize size of various nanoparticles. This measurement depends on the size of the particle core, the size of surface structures, particle concentration and the type of ions in the medium. When light hits small particles, the light scatters in all directions (Rayleigh scattering) as long as the particles are small compared to the wavelength. If the light source is a laser and thus is monochromatic and coherent, then one observes a time-dependent fluctuation in the scattering intensity. This fluctuation is due to the fact that the small molecules in solutions are undergoing Brownian motion and so the distance between the scatterers light in the solution is constantly changing with time. This scattered light then undergoes either constructive or destructive interference by the surrounding particles, and

within this intensity fluctuation, information is contained about the time scale of movement of the scatterers. DLS provide the average particle size distribution in nanofluids.

Scanning Electron Microscopy (SEM): SEM is standardized method for imaging and the measuring the dimensions of nanometer and micrometer size particles because of high imaging speed and high resolution of SEM (Buhr et al. 2009). Shah et al. (2010) the scanning electron microscope uses a focused beam of high energy electrons to generate a variety of signals at the surface of solid specimens. The signals that drive from electron sample interactions reveal information about the sample including external morphology, chemical composition and crystalline structure and orientation of materials making up the sample. However, the scanning electron microscopy does not actually view a true image of the specimen, but rather produces an electronic map of the specimen that is displayed on a cathode ray tube. Electrons from a filament in an electron gun are beamed at the specimen in a vacuum chamber. The beam forms a line that continuously sweeps across the specimen at high speed. After around 15 minutes, the beam gets stabilized and an excellent image can be captured. The SEM has a secondary electron detector. The signal produced by the secondary electrons is detected and sent to a CRT image. The scan rate for the electron beam can be increased so that a virtual 3-D image of the specimen can be viewed. Gabriel (1985) discussed about the operating conduction and operation of SEM: the basic operating condition for SEM involves high vacuum with minimum contagion, properly aligned column and saturated filament to its effective operating temperature. After setting the basic operating condition, for a given specimen the optimal imaging conditions are controlled by spot size, accelerating voltage and focus. Prepared specimen should be clean and conductive. Sometimes the filament is not heated until high vacuum is maintained. The alignment of column is evaluated, after filament has been saturated. Alignment of electron gun is evaluated in reduced

rapid or TV scan rate. In both the scanning mode, manipulate the gun X and Y electronic controls until uniform bright and centered image in CRT is obtained. SEM provides the particle size in μm or even mm sized.

Transmission Electron Microscopy (TEM): TEM is a microscopy technique whereby a beam of electron is transmitted through an ultra thin specimen, interacting with the specimen as it passes through. An image is formed from the interaction of the electrons transmitted through the specimen; the image is magnified and focused onto an imaging device, such as a fluorescent screen, on a layer of photographic film. TEMs are capable of imaging at a significantly higher resolution than light microscopes. Cullity and Stock (2001) explained the operation of TEM. TEM is a complex assembly of magnetic lenses, electron gun, a sample holder, several apertures and image viewing/ recording systems. Magnetic lenses are set into illuminating systems between sample and electron gun and those of imaging system after sample. There are three lenses in the imaging system and two condenser lenses in the illumination system. The traditional TEM mode adjusts condense lenses to illuminate the sample with approximately parallel beam. (Shah et al. 2010) as mentioned in the previous section, electrons are usually generated in an electron microscope by a process known as thermal emission from a filament, usually tungsten, in the same manner as a bulb used for light, or alternatively by field electron emission. The electrons are then accelerated by an electric potential and focused by electrostatic and electromagnetic lenses onto the sample. The beam path, the placement of the lenses, the specimen, the aperture, etc follow the plan of the light microscope. The entire arrangement, including the specimen has to be placed in high vacuum to avoid scattering and adsorption of electrons by air. Since the image is not directly viewed through an eyepiece, but is projected on a fluorescent screen on which the electrons from the image. Contrast is created by

differentiating between electrons scattered into wide angles from those scattered into small angles. The objectives aperture cuts of the larger angle electrons and the amplitude of the electron and the amplitude of the electron beam from different portions of the specimen is different leading to amplitude contrast.

X-Ray Diffraction (XRD): XRD is a rapid analytical technique primarily used for phase identification of a crystalline material and can provide information on grain size. With the help of data base of known structure XRD is used for the phase identification and XRD is also used to determine Crystal structure of unknown materials, strain, crystal size, orientation of single crystal or polycrystalline materials (Cullity and Stock 2001; Suryanarayana and Norton 1998 and Waseda et al. 2001). (Shah et al. 2010) when a crystal is bombarded with X-rays of a fixed wavelength (similar to spacing of the atomic scale crystal lattice planes) and a certain incident angles, intense reflected X-rays are produced when the wavelength of the scattered X-rays interface constructively. In order for the waves to interfere constructively, the differences in the travel path must be equal to integer multiplies of the wavelength. When this constructive interference occurs, a diffracted beam of X-rays will leave the crystal at an angel equal to that of the incident beam.

XRD is used to identify the phase and crystal structure of nanopareticles. TEM is used to measure the dimensioning of nanoparticles and gives average grain size of nanoparticles and DLS shows the average particle diameter in the mixture of basefluids and nanoparticles.

2.4 Previous Experimental investigation carried by Other Researchers

Wang et al. (1999) examined into the effective thermal conductivity of mixtures of fluids and nanometer-size particles using a steady-state parallel-plate method to measure thermal conductivity. The two types of nanoparticles Al_2O_3 and CuO dispersed in DI water, vacuum pump fluid, engine oil and ethylene glycol. The average nominal diameter of the Al_2O_3 powders was 28 nm and of CuO powders was 23 nm respectively. The thermal conductivity of nanoparticles fluid mixtures increased with decreasing particle size.

Das et al. (2003) conducted an experimental program to investigate into the thermal conductivity of nanofluids using Al_2O_3 and CuO. Particle diameter for Al_2O_3 was 38.4 nm while that for CuO was 28.6 nm with distilled water as base fluid. A temperature oscillation technique was utilized for the measurement of thermal diffusivity and thermal conductivity is calculated from it. The results indicated an enhancement of thermal conductivity of nanofluids with increase in temperature, which makes the nanofluids even more attractive for applications with high energy.

Kwak et al. (2005) investigated the thermal conductivity of CuO particles of 10-30 nm in length and ethylene glycol in conjunction with the thermal conductivity enhancement. When examined using TEM, individual CuO particles were of the shape of prolate spheroid of the aspect ratio of 3 and most of the particles were in aggregated states even after sonication for a prolonged period. From the rheological property, it has been found that the volume fraction at the dilute limit is 0.002, which is much smaller than the value based on the shape of individual particles due to the aggregation of particles. The result showed that substantial enhancement in thermal conductivity is attainable only when particle concentration is below the dilute limit.

Peterson et al. (2006) conducted an experimental investigation to examine the effect of volume fraction and temperature on thermal conductivity. Nanoparticles of copper oxide and aluminum oxide of size 29 and 36 nm, blended with distilled water in volume fraction of 2, 4, 6 and 10%, evaluated at temperature ranging from 27.5 to 34.7° C. The results indicated that the nanoparticle material, diameter, volume fraction, and bulk temperature, all have a significant impact on the effective thermal conductivity of these suspensions. The 6% volume fraction of CuO nanoparticle/distilled water suspension resulted in an increase in the effective thermal conductivity of 1.52 times than that of pure distilled water and the 10% Al_2O_3 nanoparticle/distilled water suspension increased the effective thermal conductivity by a factor of 1.3 at a temperature of 34° C.

Zhu et al. (2007) investigated the effect of different synthesis process on thermal conductvity. CuO nanofluid was synthesized by transforming an unstable $Cu(OH)_2$ precursor to CuO in water under an ultrasonic vibration, followed by microwave irradiation. The TEM image revealed needle-like particles with a width of 30-50 nm and a length of 200-300nm The influences of the type of precursor, ultrasonic vibration, microwave irradiation, and dispersant were studied. The results showed that well-dispersed CuO nanofluid with high volume fractions could be synthesized using the current method. The CuO nanofluid had a higher thermal conductivity than those prepared by the dispersing method.

Beck et al. (2009) presented new data for the thermal conductivity enhancement in seven nanofluids containing 8–282 nm diameter alumina nanoparticles in water or ethylene glycol. The

results show that the thermal conductivity enhancement in these nanofluids decreases as the particle size decreases below about 50 nm. This finding is consistent with a decrease in the thermal conductivity of alumina nanoparticles with decreasing particle size, which can be attributed to phonon scattering at the solid–liquid interface. The limiting value of the enhancement for nanofluids containing large particles is greater than that predicted by the Maxwell equation, but is predicted well by the volume fraction weighted geometric mean of the bulk thermal conductivities of the solid and liquid. This observation was used to develop a simple relationship for the thermal conductivity of alumina nanofluids in both water and ethylene glycol.

Das et al. (2009) conducted an experimental investigation to determine the thermal conductivity of three nanofluid containing aluminum oxide, copper oxide and zinc oxide nanoparticles dispersed in base fluid, (ethylene glycol and water (60:40) by mass). Particle volume fraction was up to 10% and the temperature range was 293 to 363 K. Results showed the increase in thermal conductivity as the volume fraction and temperature increases.

Mintsa et al. (2009) investigated the thermal conductivity values for three types of water-based nanofluids for various temperatures ranging between 20 and 40º C. Nanofluids considered in this paper are composed of 29 nm CuO particles as well as 36 nm and 47 nm Al_2O_3 particles. The measuring technique used is based on the transient hot wire method. Results clearly show the increase in effective thermal conductivity of nanofluids with particle volume fraction, with temperature and as well as with a reduction in particle size.

Kondaraju et al. (2010) developed an Eulerian–Lagrangian based direct numerical simulations (DNS) model was developed to investigate the effective thermal conductivity of nanofluids. A two-way coupling term to resolve the temperature interactions between the solid particles and fluid field was considered. The model also considered various forces acting on the nanoparticles. Cu/water nanofluids with 100 nm particles and Al_2O_3/water nanofluids with 80 nm particles were simulated at different volume fractions and the effective thermal conductivity of nanofluids was calculated. The present results suggest that the particle conductivity and forces acting on nanoparticle are necessary while predicting the effective thermal conductivity of nanofluids.

Hojjat et al. (2011) investigated the thermal conductivity of three nanofluid Al_2O_3 (25 nm), TiO_2 (10 nm) and CuO (30–50 nm) nanoparticles in a 0.5 wt% of carboxymethyl cellulose (CMC) aqueous solution. The thermal conductivity of nanofluids showed no significant enhancement for nanoparticles concentrations up to 1.5 vol%. This may be due to the high apparent viscosity of nanofluids. However, at higher nanoparticles concentrations (3 and 4% volume concentration), the thermal conductivities of CuO and TiO_2 nanofluids are remarkably higher than that of the base fluid. This may be due to the reduction of interparticle distances and the creation of chain-like structures of nanoparticles.

Wang Wie et al. (2012) In this work, a comprehensive model to predict large enhancement of thermal conductivity of nanofluids by considering the graded nanolayer, the mutual interaction of spherical nanoparticles and the Brownian motion is proposed. The model investigates the relationship between the enhanced thermal conductivity and nanoparticle size, nanolayer thickness, the interaction of adjacent nanoparticles, volume fraction and temperature.

Furthermore, the theoretical results on the effective thermal conductivity of nanofluids are in good agreement with that of experimental data.

Calvin et al. (2013) studied nanoparticles Brownian motion contributes to the effective thermal conductivity of nanoparticle suspension and also compared the theoretical predictions with the results of experimental data for Al_2O_3. The results presents a comparison of the theoretical predictions obtained using this model with theof experimental results obtained for Al_2O_3/ethylene glycol suspensions at room temperature, T =300 K, and a nanoparticle velocity U =0.301 m/s and $\alpha=k_p/k_f$ =140.625. Here the contribution of the critical volume fraction is *Pe(*0.060777*)* = 0.0802. Here, it shows that smaller diameter nanoparticles lead to a greater enhancement on effective thermal conductivity and also show that with the same experimental setup, the 33 nm nanoparticle suspensions has the highest enhancement on effective thermal conductivity, then 28 nm nanoparticles suspension and finally the 38 nm nanoparticle suspension has the smallest enhancement. The comparison show that transient hot wire method gave greater enhancement on effective thermal conductivity of nanoparticles suspension than steady state method and with 5 nm difference in naonparticles diameters the difference in the enhancement would be very huge in transient hot wire method.

Wenhua Yu et al. (2013) studied a distribution-based modeling technology for the effective thermal conductivity of carbon nanotube-based nanofluids was proposed, from which several predictive equations for the effective thermal conductivity of carbon nanotube-based nanofluids were derived. These predictive equations capture key factors in the effective thermal conductivity modeling of carbon nanotube based nanofluids, i.e., the effects of carbon nanotube

curving and wrapping. Comparisons between the theoretical predictions and the experimental data were presented for carbon nanotubes suspended in four base fluids. The results show that most of the experimental data fall within the lower bound set by the linear decrease distribution model and the upper bound set by the linear increase distribution model and that the most of the experimental data can be predicted by the combination of the uniform distribution model and the linear increase distribution model.

CHAPTER 3: EVALUATION OF EXISTING MODELS FOR THERMAL CONDUCTIVITY OF NANOFLUIDS

To evaluate the accuracy of the existing theoretical and empirical models for the thermal conductivity of nanofluids, the same have been evaluated in this chapter against a wide range of experimental data for Copper oxide-based nanofluids, till now no one researchers evaluate the models against copper oxide-based nanofluids. Equation 3.1 to 3.3 is theoretical models and equation 3.4 and 3.5 are empirical.

3.1 Murshed et al. (2008)

Murshed et al. (2008) developed the models by considering the contribution of interfacial layer at the solid-liquid interface on the effective thermal conductivity of nanofluids. It was assumed that the liquid (base fluid), interfacial layer and solids collectively form nanofluids; all the nanoparticles which are stationary are separated from each other; there is a continuous heat flux at interfaces like layer/fluid and particle/layer. Interfacial layer thickness is taken as 1 nm (Murshed et al., 2008) for the purpose of calculation in this paper. Following equation (3.1) is for the effective thermal conductivity of nanofluids with spherical nanoparticles and $K_{lr} = 3\ K_f$:

$$K_{nf} = \frac{(K_p - K_{lr})\phi K_{lr}(2\varepsilon_1^{\ 2} - \varepsilon^3 + 1) + (K_p + 2K_{lr})\varepsilon_1^{\ 3}\{\phi\varepsilon^3(K_{lr} - K_f) + K_f\}}{(K_p + 2K_{lr})\varepsilon_1^{\ 3} - (K_p - K_{lr})\phi_p(\varepsilon_1^{\ 3} + \varepsilon^3 - 1)} \tag{3.1}$$

$$Where, \varepsilon = 1 + \frac{\delta}{r}; \varepsilon_1 = 1 + \frac{\delta}{2r}$$

3.2 Xie et al. (2005)

Xie et al. (2005) considered the effect of thermal conductivity enhancement due to interfacial nanolayer at the liquid-solid interface with thermal conductivity distribution is linear. This model also considered particle size, particle distribution, thermal conductivity of basefluid and nano

particle. The model is given by equation 3.2. The model is used for low volume fractions of nanoparticles in base fluids (Xie et al., 2005).

$$\frac{K_{nf} - K_f}{K_f} = 3\Theta\phi_T + \frac{3\Theta^2\phi_T^{\,2}}{1 - \Theta\Phi_T} \tag{3.2}$$

Where, Θ, B_{lf}, B_{pl}, B_{fl}, K_l,Φ_T and M are defined by:

$$\Theta = \frac{B_{lf}\left[(1+\gamma)^3 - \frac{B_{pl}}{B_{fl}}\right]}{(1+\gamma)^3 + 2B_{pl}B_{lf}}; B_{pl} = \frac{K_p - K_l}{K_p + 2K_l}; B_{fl} = \frac{K_f - K_l}{K_f + 2K_l}; B_{lf} = \frac{K_l - Kf}{K_l + 2K_f}$$

$$K_l = \frac{K_f M^2}{(M-\gamma)\ln(1+M) + \gamma M}; \phi_T = \varphi(1+\gamma)^3; \gamma = \frac{\delta}{r_p}; M = \alpha(1+\gamma) - 1$$

3.3 Yu and Choi (2003)

In this model, Maxwell's model (Maxwell 1873) was modified by considering the effect of ordered liquid nano-layer around the nanoparticles on the thermal conductivity of nanofluids. Nano-layer had an effect on thermal conductivity of nanofluids when diameter of nanoparticles is less than 10 nm (Yu and Choi, 2003).

$$\frac{K_{nf}}{K_f} = \frac{K_p + 2K_f + 2(K_p - K_f)(1+\gamma)^3\phi}{K_p + 2K_f - (K_p - K_f)(1+\gamma)^3\phi} \tag{3.3}$$

3.4 Mintsa et al. (2009)

By using simple regression analysis with R^2 value of 95%, the empirical model was developed for the ratio of thermal conductivity of CuO-water nanofluid. The relative thermal conductivity of nanofluids directly influenced to the volume fraction. The following equation 3.4 shows the empirical model for the CuO/water.

$$\frac{K_{nf}}{K_f} = 1.74\phi + 0.99 \tag{3.4}$$

3.5 Peterson et al. (2006)

This empirical model was developed by two factor linear regression analysis for thermal conductivity ratio of CuO-water. This ratio is a function of different volume fraction and temperature. The equation 3.5 show the empirical model with R^2 value of 0.907 is

$$\frac{K_{nf}}{K_f} = 3.761088\phi + 0.017924t - 0.30734 \tag{3.5}$$

3.6 Evaluation of models for CuO nanofluids

The above theoretical and empirical models have been evaluated, by using them to predict the ratio of thermal conductivity of nanofluids to that of base fluids for a range of experimental conditions and comparing them with available experimental data for the same range of volume fraction, temperature and particle size. Following are the characteristics of nanoparticles and basefluid used in this study:

Table 3.1: Physical Properties of CuO-Water Nanofluids

Reference	**Particle average diameter (nm)**	**Volume fraction (%)**	**Temperature (°C)**
Zhu et al. (2011)	10	0.1 to 0.8	25

Gilles et al. (2009)	29	6	21 to 26
Gilles et al. (2009)	29	9	22 to 28
Das et al. (2003)	28.6	1 to 4	51
Das et al. (2003)	28.6	1	20 to 42
Das et al. (2003)	28.6	1 to 4	36
Hojjat et al. (2011)	40	0.1 to 1	15

1) Particle density of CuO 6500 Kg/m^3 (Das et al., 2009).

2) Thermal conductivity of CuO is 17.65 W/mK (Das et al., 2009).

3) Thermal conductivity of water varies from 0.57 W/mK at 0 °C to 0.67 W/mK at 100 °C (Das et al., 2009).

In Figure 3.1, values of experimental thermal conductivity ratio for CuO nanoparticle diameter of 10 nm and at 25^{o}C temperature have been compared with predictions obtained using theoretical models for a range of nanoparticle volume fractions.

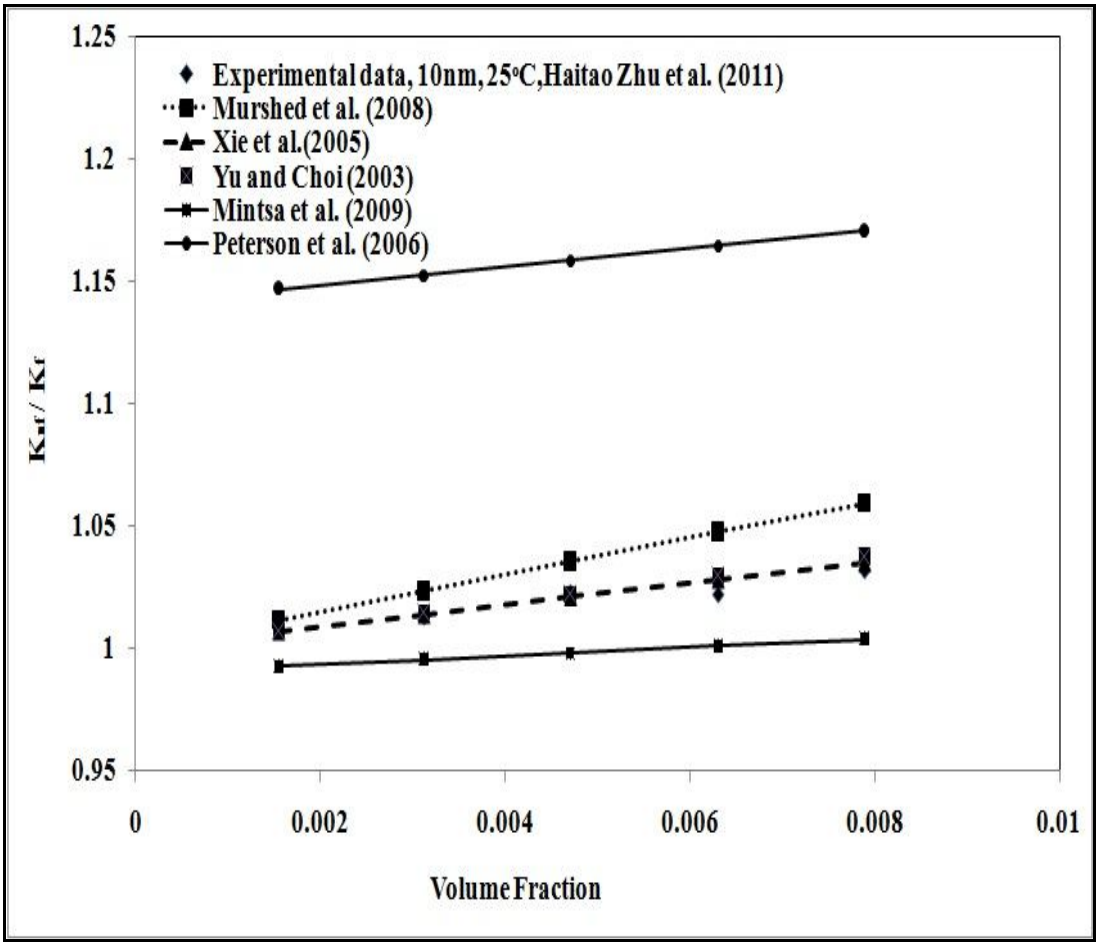

Figure 3.1: Experimental versus predicted values of thermal conductivity ratio with increase in volume fraction of CuO nanoparticles, d: 10 nm, T: 25^{o}C

In Figure 3.1, the thermal conductivity ratio of predicted with theoretical and empirical models are compared with experimental data (Zhu et al. 2011) of thermal conductivity ratio having a particle diameter 10 nm and at a temperature of 25°C for a given range of volume fraction. The thermal conductivity ratio of experimental and predicted values of Xie et al. (2005) and Yu and Choi (2003) are overlapping in the given volume fraction range. Murshed et al. (2008) and Mintsa et al.(2009) show over-and under-predicting thermal conductivity ratio to the experimental respectively because, minsta et al. 2009 considered only volume fraction in the model.

In Figure 3.2, the thermal conductivity ratio of predicted with theoretical and empirical models are compared with experimental data of thermal conductivity ratio having a particle diameter 29nm at a constant volume fraction 0.0612 for a given temperature range.

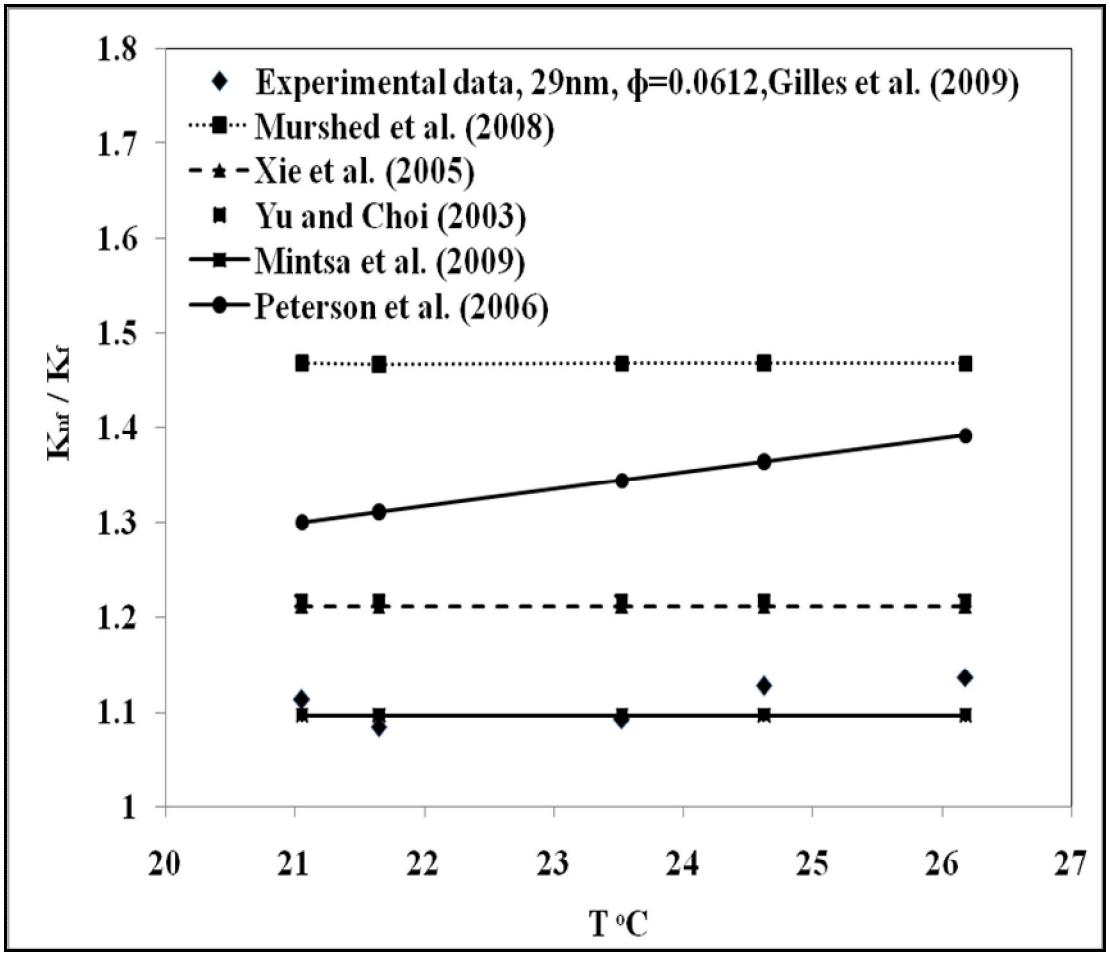

Figure 3.2: Experimental versus predicted values of thermal conductivity ratio with increase in temperature of CuO nanoparticles, d: 29 nm, □: 0.061

The thermal conductivity ratio of experimental and Mintsa et al. (2009) provided similar results up to 23.5°C and after this temperature, Mintsa et al. (2009) shows under predictions to experimental data. Predictions of Yu and Choi (2003) and Xie et al. (2005) are found to be overlapping and show over-predicted to experimental thermal conductivity ratio.

In Figure 3.3, the thermal conductivity ratio of predicted with theoretical and empirical models are compared with experimental data Mintsa et al. (2009) of thermal conductivity ratio having a particle diameter of 29nm at a constant volume fraction of 0.093 for a temperature range of 22°C to 28°C.

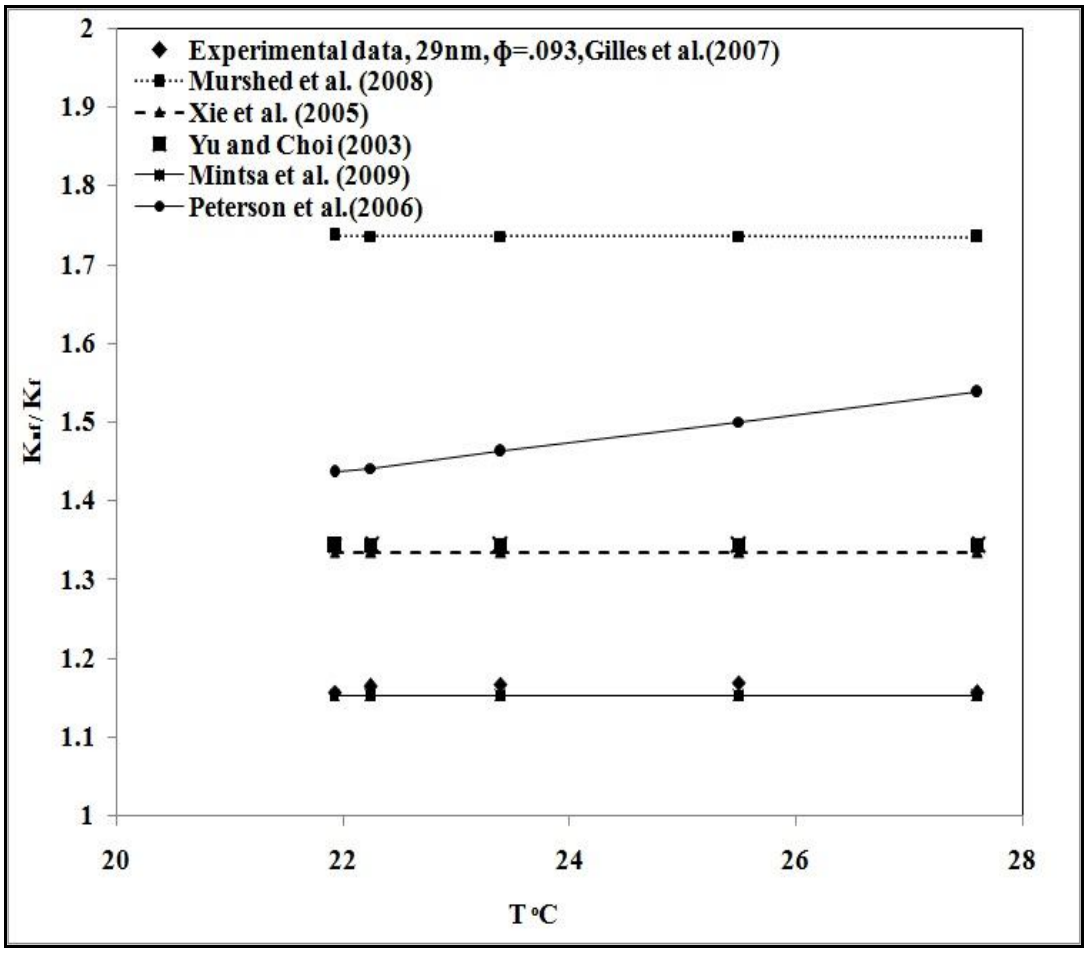

Figure 3.3: Experimental versus predicted values of thermal conductivity ratio with increase in temperature of CuO nanoparticles, d: 29 nm, □=0.093

Figure 3.3 shows thermal conductivity ratio of Yu and Choi (2003) and Xie et al. (2005) over predicted to experimental data and also overlapping occur. Peterson et al. (2006) shows over predicted to experimental values Mintsa et al. (2009) and experimental data of thermal

conductivity ratio are overlapping. Inaccuracy rate increases more in Peterson et al. (2006) as temperature increases.

In Figure 3.4, the thermal conductivity ratio of predicted with theoretical and empirical models are compared with experimental data (Das et al. 2003) of thermal conductivity ratio having a particle diameter 28.6nm and a temperature of 51°C for a given range of volume fraction.

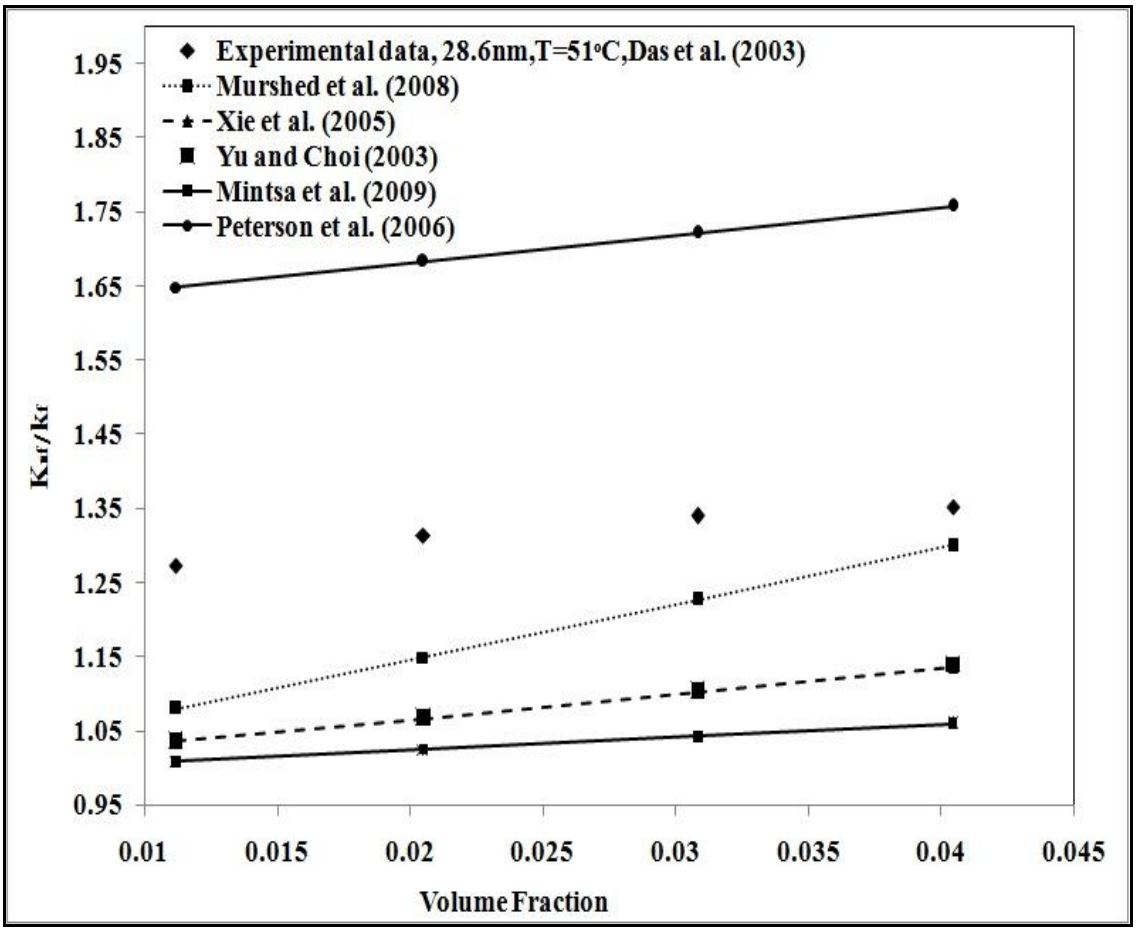

Figure 3.4: Experimental versus predicted values of thermal conductivity ratio with increase in volume fraction of CuO nanoparticles, d: 28.6 nm, T: 51^{o}C

The thermal conductivity ratio of all theoretical and empirical models is under predicted to experimental data except Peterson et al., (2006). Thermal conductivity ratio starts converging as

the volume fraction increases from (0.01-0.04) for all models except Peterson et al., (2006) and also shows highest over prediction values to the experimental.

In Figure 3.5, the thermal conductivity ratio of predicted with theoretical and empirical models are compared with experimental data (Das et al. 2003) of thermal conductivity ratio having a particle diameter 28.6 nm at a constant volume fraction of 1% for a temperature range of 20°C to 42°C.

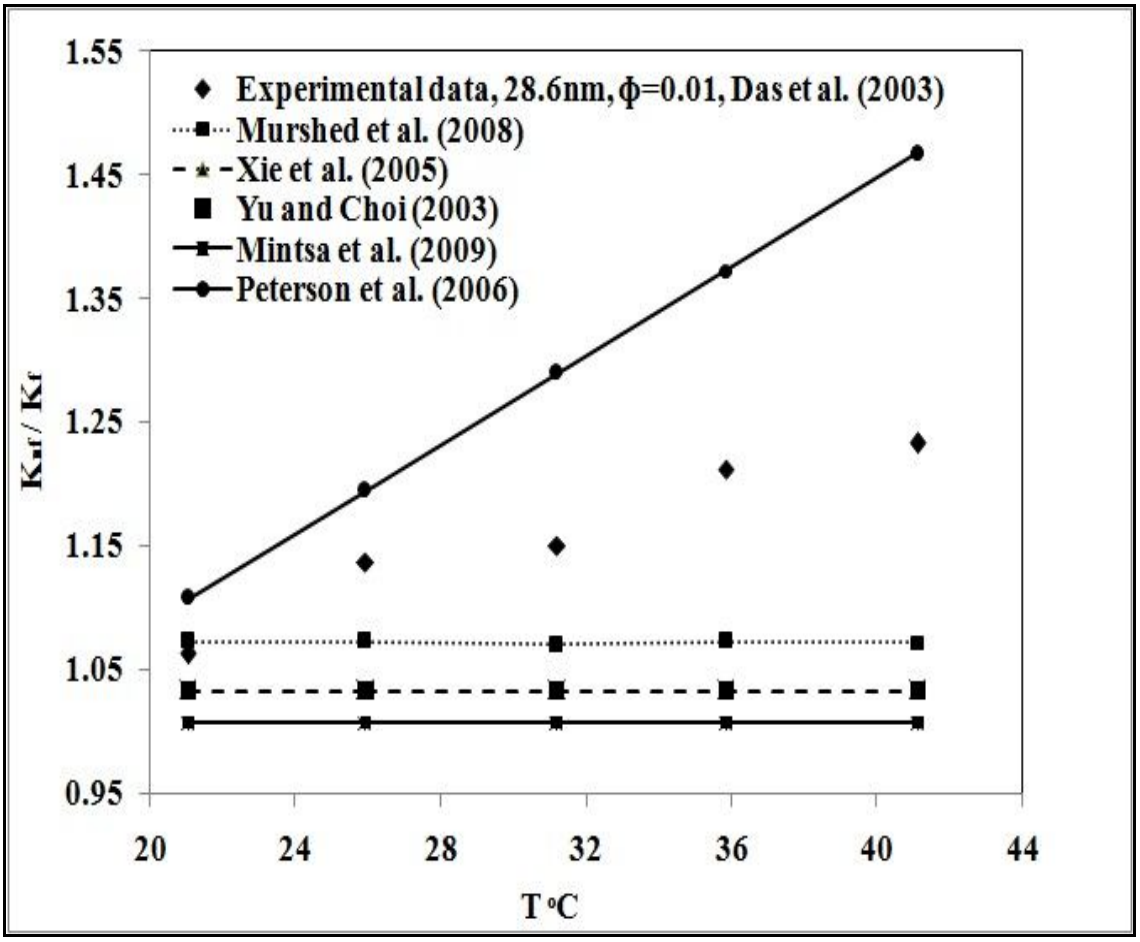

Figure 3.5: Experimental versus predicted values of thermal conductivity ratio with increase in temperature of CuO nanoparticles, d: 28.6 nm

Mintsa et al. (2009) shows lowest under-predicted values to the experimental data. All models show under predicted values to the experimental data except Peterson et al. (2006). Thermal

conductivity ratio of Peterson et al. (2006) starts diverging as the temperature increases because, Peterson et al. (2006) considered temperature and volume fraction parameters two parameters to model the thermal conductivity of nanofluids, so as the temperature increases thermal conductivity of nanofluids increases for Peterson et al. (2006) model

In Figure 3.6, values of experimental thermal conductivity ratio for CuO nanoparticle diameter of 28.6 nm and at 36^{o}C temperature have been compared with predictions obtained using theoretical models for a range of nanoparticle volume fractions.

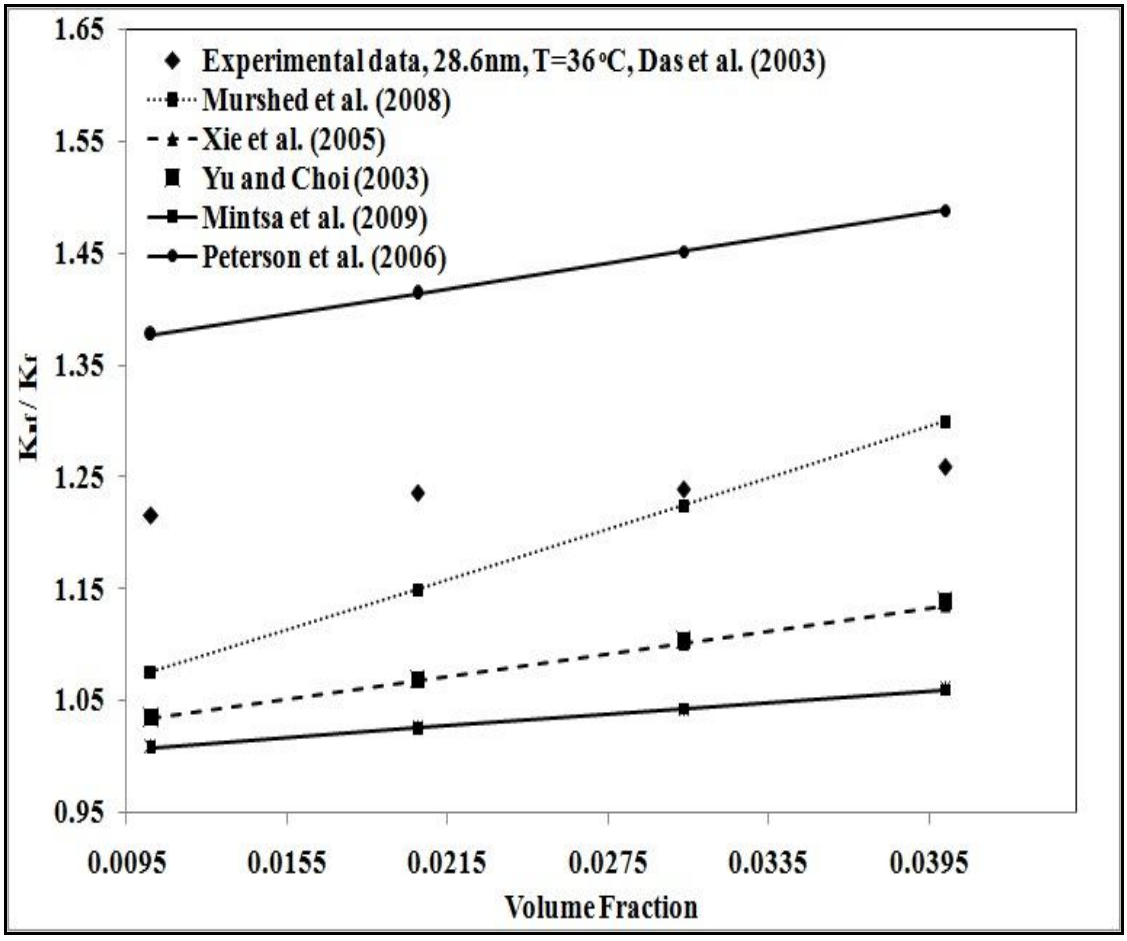

Figure 3.6: Experimental versus predicted values of thermal conductivity ratio with increase in volume fraction of CuO nanoparticles, d: 28.6 nm, T=36 □C

As the volume fraction increases, the thermal conductivity ratio starts converging for all theoretical and empirical models. After volume fraction of 0.0305, thermal conductivity ratio of Murshed et al. (2008) over predicted to experimental data. Peterson et al. (2006) shows highest over prediction to the experimental data.

In Figure 3.7, the thermal conductivity ratio of predicted with theoretical and empirical models are compared with experimental data (Das et al. 2003) of thermal conductivity ratio having a particle diameter of 28.6nm and a temperature of 21 □C for a given range of volume fraction.

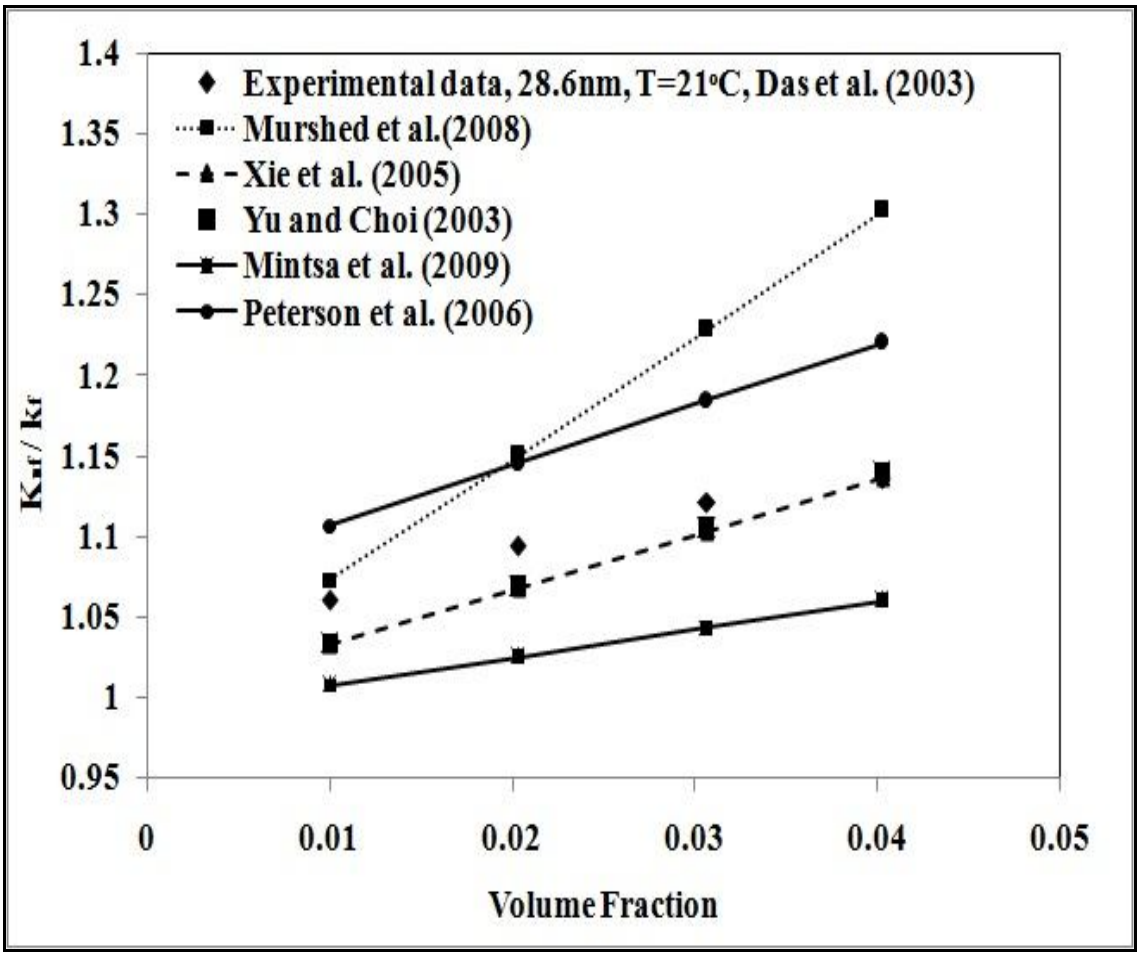

Figure 3.7: Experimental versus predicted values of thermal conductivity ratio with increases in volume fraction of CuO nanoparticles with diameter 28.6nm, T=21°C

The thermal conductivity ratio of Peterson et al. (2006) and Mintsa et al. (2009) show over and under predicted to the experimental values respectively. The thermal conductivity ratio of Mintsa et al. (2009) show very close to experimental values at volume fraction 0.01 and as the volume fraction increases the conductivity ratio start diverging. Xie et al. (2005) and Yu and Choi (2003) start superimposing as volume fraction increases.

In Figure 3.8, the thermal conductivity ratio of predicted models are compared with experimental data (Hojjat et al. 2011) of thermal conductivity ratio having a particle diameter of 40 nm and a temperature of 15°C given range of volume fraction.

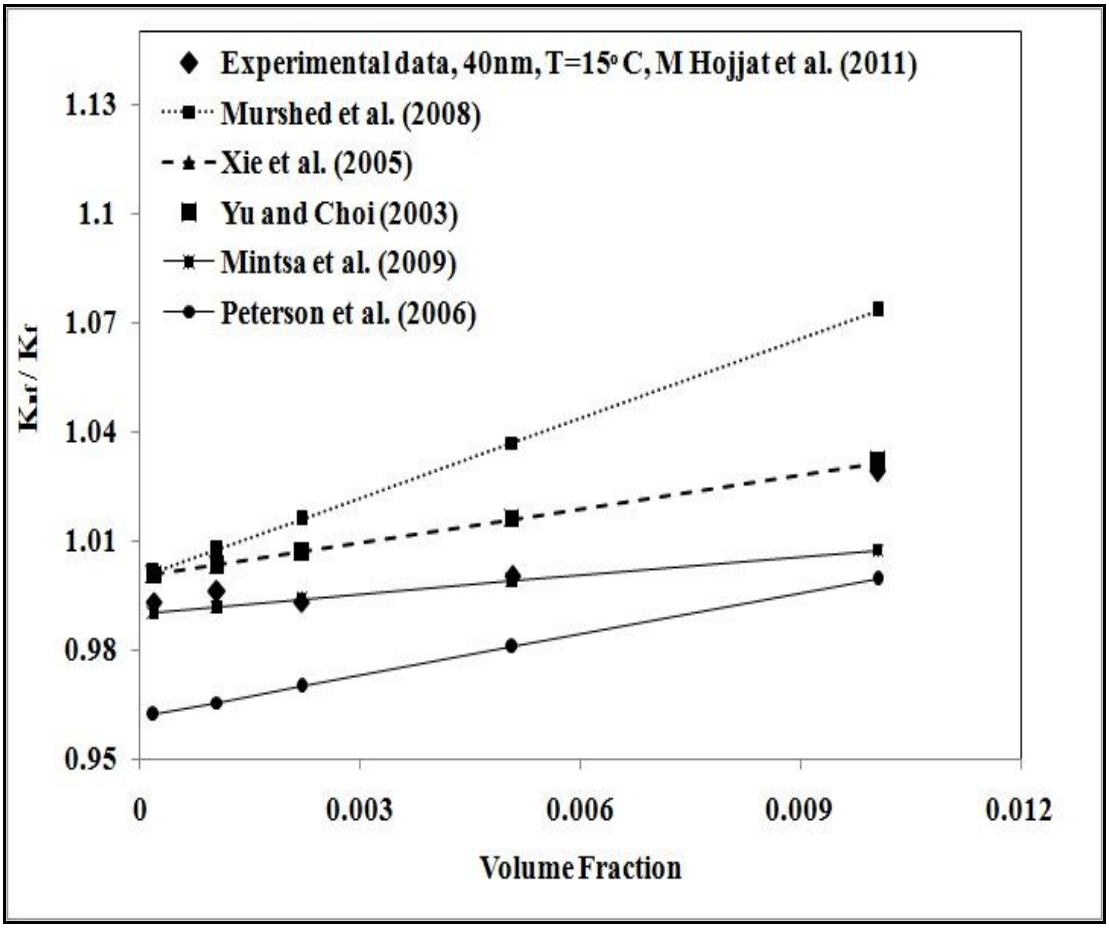

Figure 3.8: Experimental versus predicted values of thermal conductivity ratio with increases in volume fraction of CuO nanoparticles with diameter 40nm, T=15°C

At low volume fraction, Peterson et al. (2006) show under predicted to experimental thermal conductivity ratio and start converging as volume fraction increases. The values of Mintsa et al. (2009) are overlapping with the experimental data. At low volume fraction, Murshed et al. (2008) show thermal conductivity ratio close to experimental data but start diverging as volume fraction increases.

Table 3.2 provides average sum of relative error for thermal conductivity ratio (using the formula given below) to indicate the prediction accuracies of the different models (Figure 3.1 to 3.8).

$$\text{Relative error} = \sum_{n} \left| \frac{\text{experimental value - predicted value}}{\text{experimental value}} \right| \times 100\%$$

Table 3.2: Relative Errors of Model Predictions (%)

Figure No.	**Murshed et al., (2008)**	**Xie et al., (2005)**	**Yu and Choi (2003)**	**Mintsa et al., (2009)**	**Peterson et al., (2006)**
3.1	1.54	0.17	0.32	2.14	13.61
3.2	32.25	9.16	9.66	1.86	20.93
3.3	49.31	14.81	13.49	0.89	26.93
3.4	9.96	17.77	17.60	21.59	29.05
3.5	7.61	10.66	10.59	12.85	10.73
3.6	5.74	14.21	12.22	16.46	15.75
3.7	7.62	1.68	1.64	6.23	5.52
3.8	2.46	0.93	.95	.59	2.66
Mean of error	14.56	8.67	8.30	11.49	15.64

CHAPTER 4: EXPERIMENTAL EVALUATION OF THERMAL CONDUCTIVITY

4.1 Experiment

Nanometer-size ZnO, single wall carbon nanotubes (SWCNT) and Ag nanoparticles which is colloidal solution in water are obtained from Reinste Nano Ventures Private Limited (Noida). The average diameter of ZnO powders 14 nm and 25 nm with 1 nm surfactant coating of oleic acid. The density of single wall carbon nanotubes is 0.05 g/cm^3 and the average diameter of SWCNT shows in TEM image Figure 4.1.

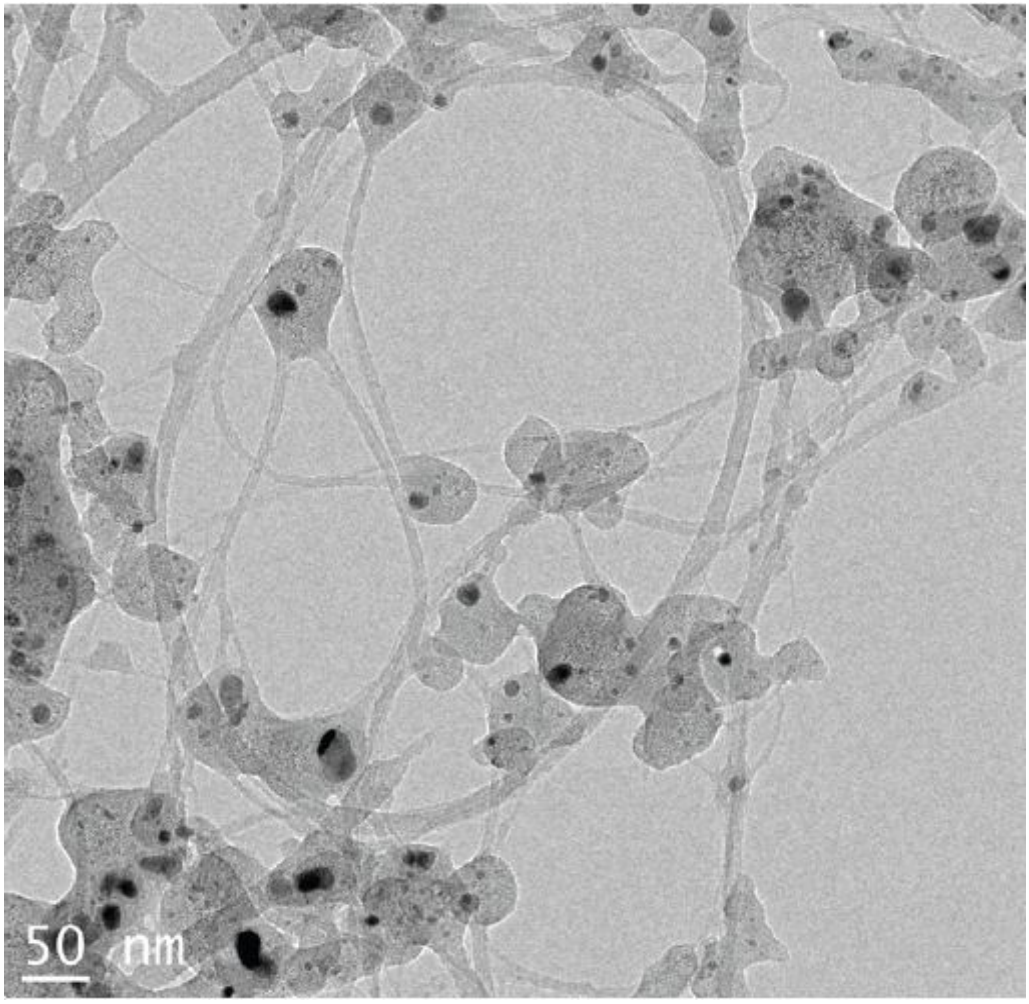

Figure 4.1: TEM image of Single Wall Carbon Nanotubes

4.2 Nanofluid synthesis

The as-received powders are sealed, dry and loosely agglomerated. Particle density of ZnO is 5600 kg/m^3 and thermal conductivity is 13 W/mK (Das et al., 2009). Two step method was used to prepare the ZnO based nanofluids of two different volume fraction 0.01% and 0.05%. The amount of powder for 0.01% volume fraction and 0.05% volume fraction are 11.2 mg and 56 mg respectively and then dispersed in 20 ml of DI water and ethylene glycol basefluids and compare the relative thermal conductivity of both ZnO DI water and ethylene glycol based nanofluids. The prepared samples are blended by ultrasonic bath sonicator for different sonication time (0, 2, 4, 6 and 8 hours) the thermal conductivity of ZnO based nanofluid at different sonication and settling time of both 14 nm and 25 nm size of ZnO nanopowder were measured. The 2 hours gap considered sufficient time to measure thermal conductivity of nanofluid of next sample because, for one sample reading it takes 90 minute. As received single wall carbon nanotubes powder agglomerated so to prepare SWCNT nanofluids, firstly single wall carbon nanotubes grinded mechanically and magnetic stirrer is used for better mixing of nanopowders in basefluid as shown in Figure A1 and then samples were sonicated in ultra probe sonicator. At volume fraction 4% of aqueous silver nanoparticles were suspended in DI water basefluids and sonicated in ultra probe sonicator as shown in Figure 4 A2.

Thermal conductivity data were measured in all case using the Decagon devices KD2 Pro Thermal Properties Analyzer (Decagon Devices Inc., Pullman, WA, USA). This apparatus meets the standards of ASTM D5334 and IEEE 442-1981 regulations. Its principle of measurement is based on the transient hot-wire source approach and the thermal probe, containing a heating element and a thermoresistor, is to be inserted into the sample vertically. A single reading takes 120 seconds. The first 90 s are used to ensure temperature stability, after which the probe is heated for 30 s using a controlled current intensity. The thermistor measures the changing

temperature while the microprocessor stores the data. Three readings were taken at each volume fraction, after each reading 15 more minutes were allowed to pass before carrying out the next measurement to ensure complete thermal equilibration as recommended by kd2 pro company. The reading given by the KD2 pro instrument is main issue because, data is non reproducible and the instrument is very sensitive to any disturbance during measurement of thermal conductivity of nanofluids so, to avoid the disturbance in measuring thermal conductivity of nanofluids the table was isolated from vibration by installing vibration isolation pads and fan also switched off. Figure 4 A3, shows the experimental setup of measuring thermal conductivity of ZnO nanofluids.

Before analysis of the nanofluid samples, the accuracy of the probe was carefully calibrated on DI water of well known thermal conductivity, (standard values available in literature). The thermal conductivity were measured with the KD2 Pro instrument at different temperatures 17, 21and 25° C and calibrated with the expected values of thermal conductivity. Figure 4.5 shows expected thermal conductivity versus measured thermal conductivity of DI water.

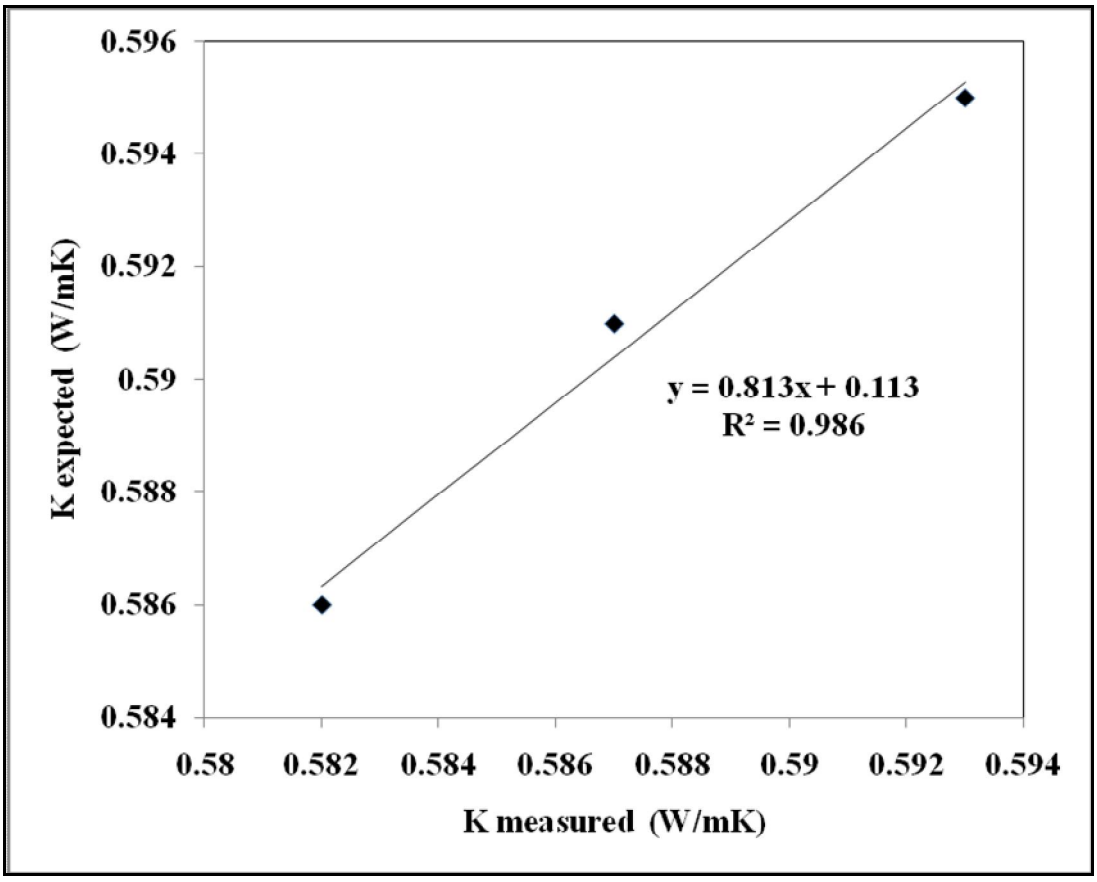

Figure 4.5: Expected versus measured thermal conductivity of DI water at different temperatures

The trend for these data points is straight line and resulted best fit with R^2 value is 0.986.

In Figure 4.6, the effect of sonication time was investigated on thermal conductivity ratio of ZnO based nanofluids for different nanoparticles sizes of 14 and 25 nm at volume fraction of 0.01% and 0.05%.

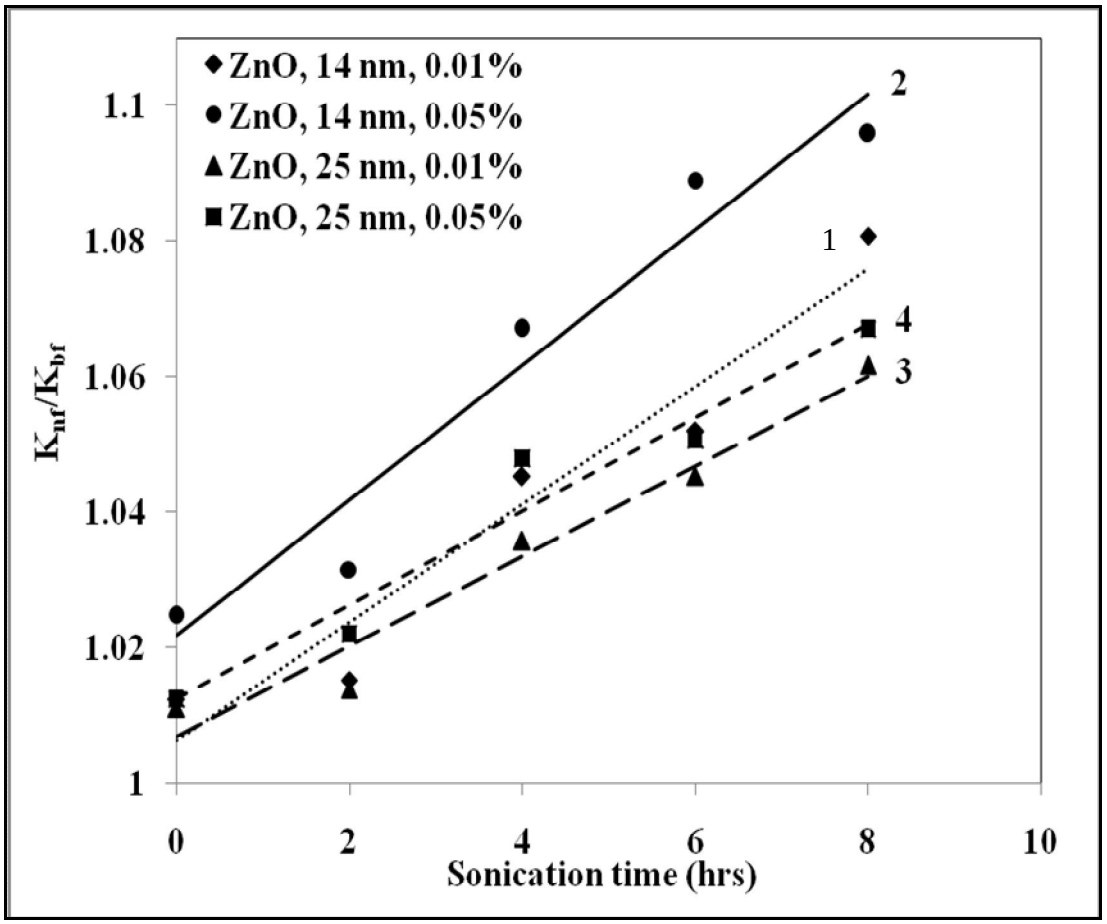

Figure 4.6: Thermal conductivity ratio variation with sonictation time at different particle size and volume fraction of ZnO nanoparticle, T=25°C

In Figure 4.6, line 1: and line 2: show the linear trend of ZnO nanoparticles, with particle diameter of 14 nm at 0.01% and 0.05% volume fractions respectively. Line 3: and line 4: show the linear trend of ZnO nanoparticles with particles diameter of 25 nm at 0.01% and 0.05% volume fractions, respectively. In Figure 4.6, the relative thermal conductivity of ZnO nanofluid increases as the sonication time increases because, as the sonication time increases, nanoparticles of ZnO were dispersing more, which provided more surface to volume ratio. Therefore, thermal conductivity increases as the surface to volume increases because the conductivity is surface phenomenon. For particle diameter of 14 nm, the thermal conductivity increases as the volume

fraction increases from 0.0001 to 0.0005 because the thermal conductivity of solid particles more than liquid so, as the concentration of nanoparticles increases thermal conductivity also increases. As the concentration rises, the formation of chain structure has been seen.

In Figure 4.7, the effect of settling time investigated on thermal conductivity ratio of ZnO based nanofluids of different sizes 14 nm and 25 nm at volume fraction 0.01% and 0.05%

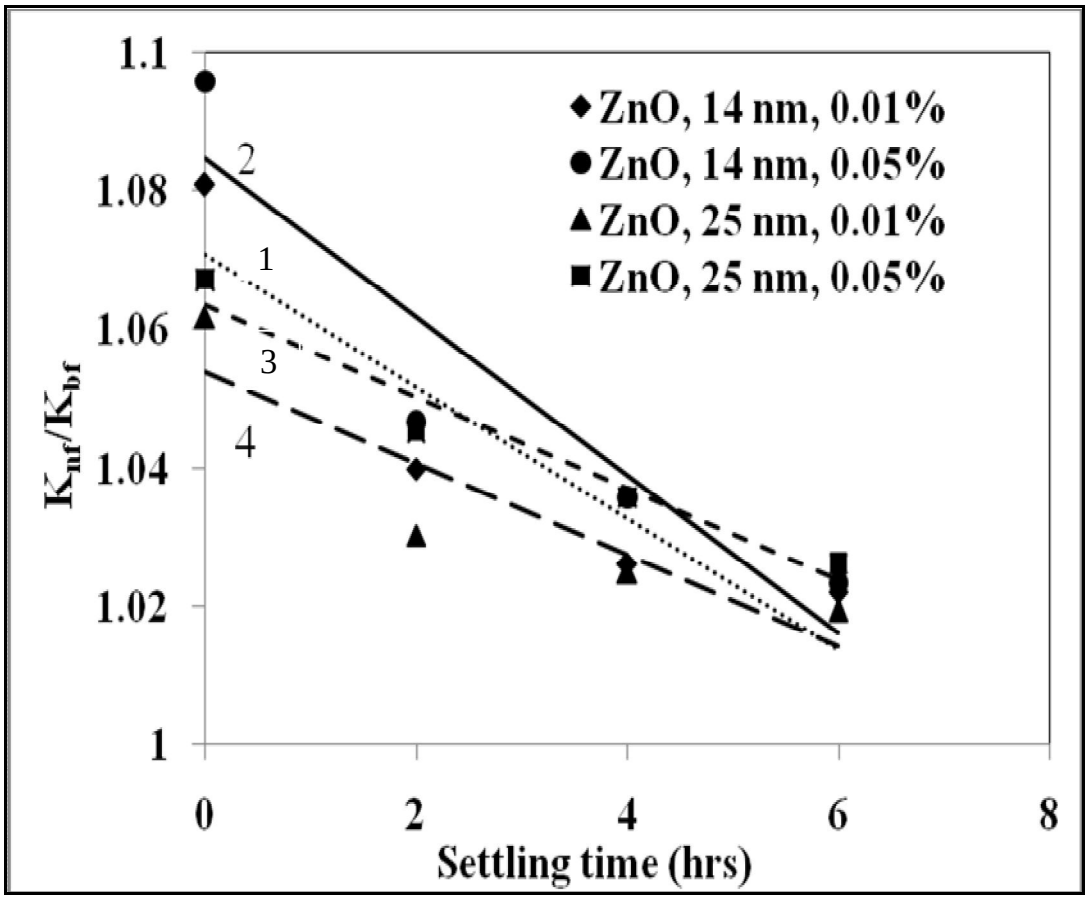

Figure 4.7: Thermal conductivity ratio variation with settling time at different particle size and volume fraction of ZnO nanoparticle, T=25°C.

In Figure 4.7, line 1: and line 2: shows the linear trend of ZnO nanoparticles, diameter of 14 nm at 0.01% and 0.05% volume fractions respectively. Line 3: and line 4: shows the linear trend of ZnO nanoparticles, diameter of 25 nm at 0.01% and 0.05% volume fractions respectively. The

samples were prepared by dispersing nanoparticles in ultra bath sonicator up to 8 hours. The thermal conductivity ratio of ZnO nanofluid decreases as the settling time increases because, as the time increases the nanoparticles which were dispersed in basefluid, starts agglomerated due to which cluster formation visualize and settle down as the time increases

In Figure 4.8, shows the effect of temperature on thermal conductivity ratio of ZnO nanofluid for different diameter 14 nm and 25 nm at constant volume fraction 0.05%.

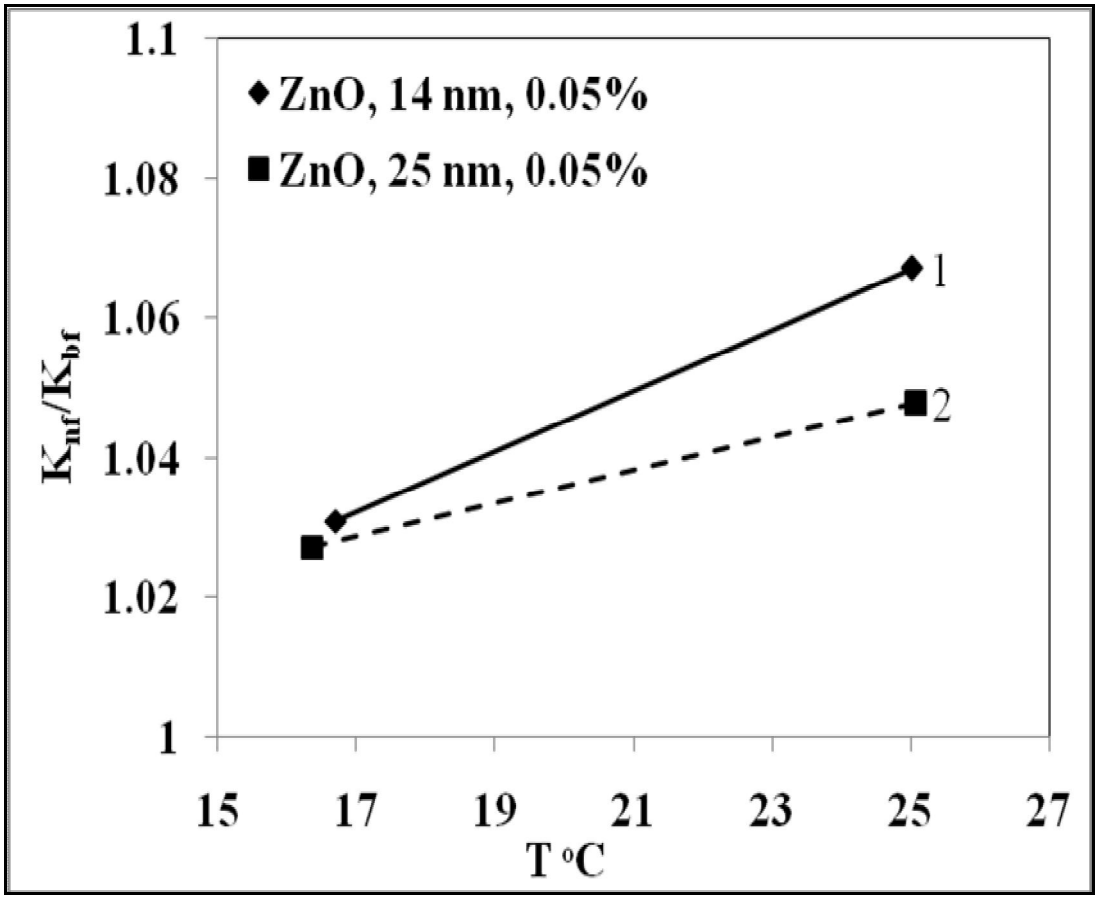

Figure 4.8: Thermal conductivity ratio variation with temperature for 14 nm and 25 nm diameter at 0.05% volume fraction.

In Figure 4.8, line 1: and line 2: show the variation of ZnO nanofluid of diameter 14 nm and 25 nm respectively at 0.05% volume fraction. The samples were sonicated up to 4 hours. The thermal conductivity ratio of ZnO nanofluids for both 14 nm and 25 nm diameters of

nanoparticles rise because, as the temperature increases Brownian motion of nanoparticles increase. As a result, the particles get excited due to which random motion of nanoparticles increases and the particles starts strike with each other and transfer the heat energy.

In Figure 4.9, the effect of sonication time was investigated on thermal conductivity ratio of ZnO based nanofluids (Ethylene Glycol) for different nanoparticles sizes of 14 and 25 nm at volume fraction of 0.01% and 0.05%.

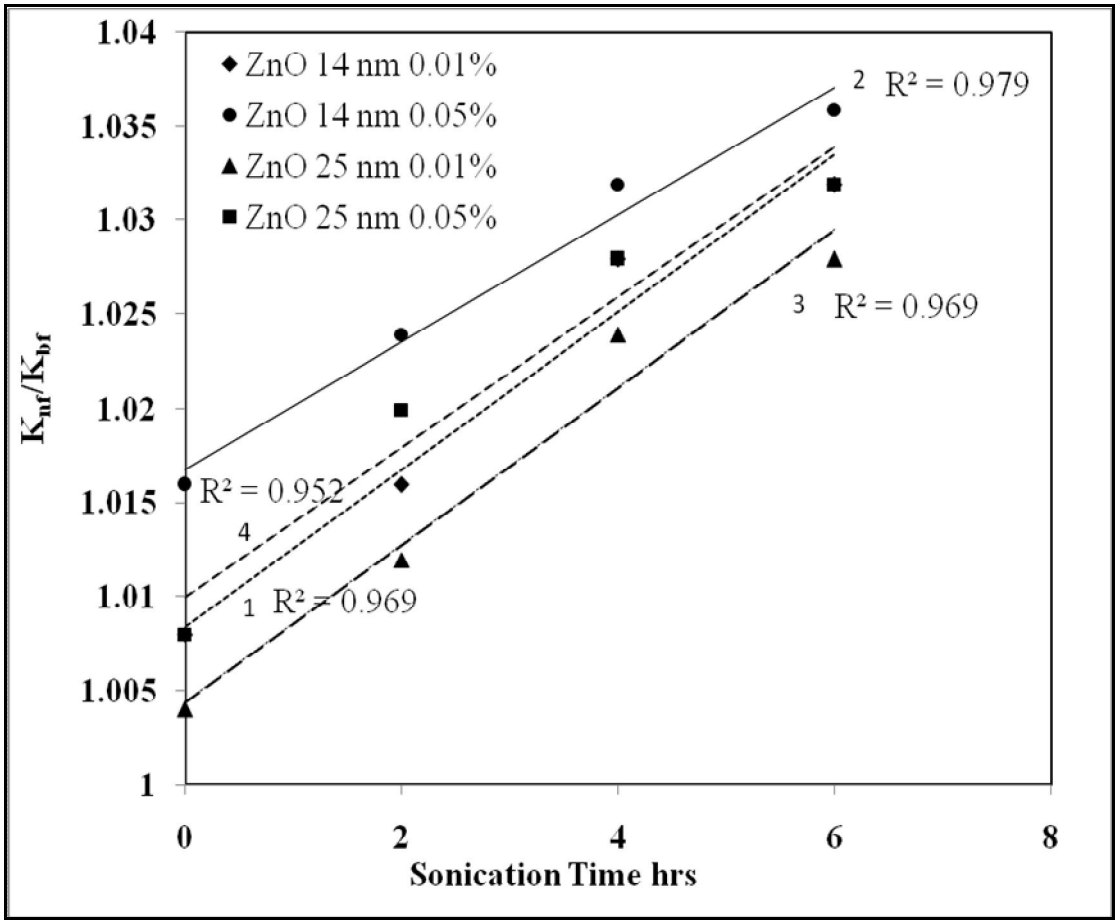

Figure 4.9: Thermal conductivity ratio variation with sonication time at different particle size and volume fraction of ZnO nanoparticle, T=25°C

In Figure 4.9, line 1: and line 2: shows the linear trend of ZnO nanoparticles, diameter of 14 nm at 0.01% and 0.05% volume fractions respectively. Line 3: and line 4: shows the linear trend of

ZnO nanoparticles, diameter of 25 nm at 0.01% and 0.05% volume fractions respectively. The samples were prepared by dispersing ZnO nanoparticles into the ethylene glycol basefluid. The thermal conductivity ratio of nanofluid to basefluid increases as the sonication time increases and also as the diameter of nanoparticles increases relative conductivity of ZnO nanoparticles decreases this is because, surface to volume ratio decreases.

In Figure 4.10, the effect of settling time investigated on thermal conductivity ratio of ZnO based nanofluids of different sizes 14 nm and 25 nm at volume fraction 0.01% and 0.05%.

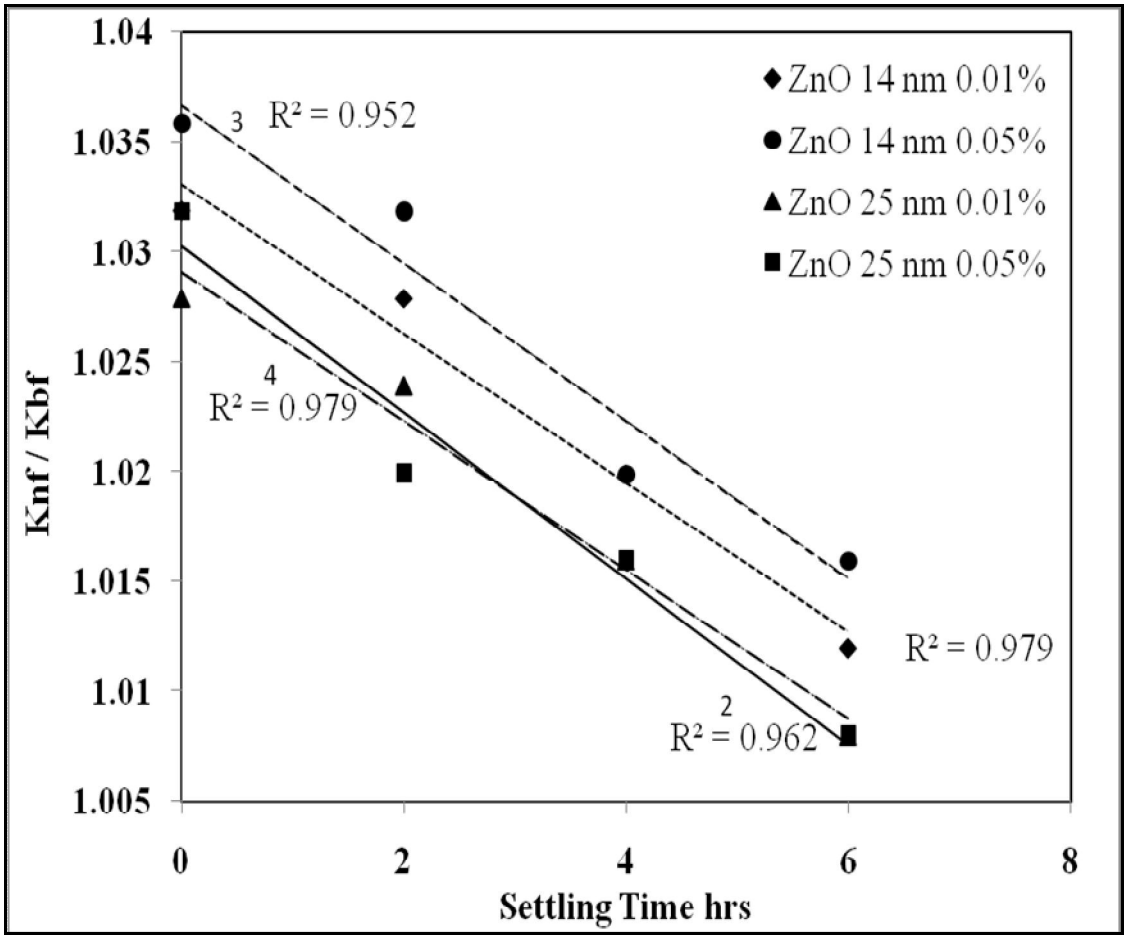

Figure 4.10: Thermal conductivity ratio variation with settling time at different particle size and volume fraction of ZnO nanoparticle, T=25°C.

In Figure 4.10, line 1: and line 2: shows the linear trend of ZnO nanoparticles, diameter of 14 nm at 0.01% and 0.05% volume fractions respectively. Line 3: and line 4: shows the linear trend of ZnO nanoparticles, diameter of 25 nm at 0.01% and 0.05% volume fractions respectively. The ZnO nanoparticles dispersed in ethylene glycol basefluids. The effective thermal conductivity of ZnO nanoparticles based nanofluids decreases, as the settling time increases. The trend for these data points is straight line and resulted best fit with R^2 value show in Figure 4.10.

In Figure 4.11, shows the effect of temperature on thermal conductivity ratio of ZnO (ethylene glycol as basefluid) nanofluid for different diameter 14 nm and 25 nm at constant volume fraction 0.05%.

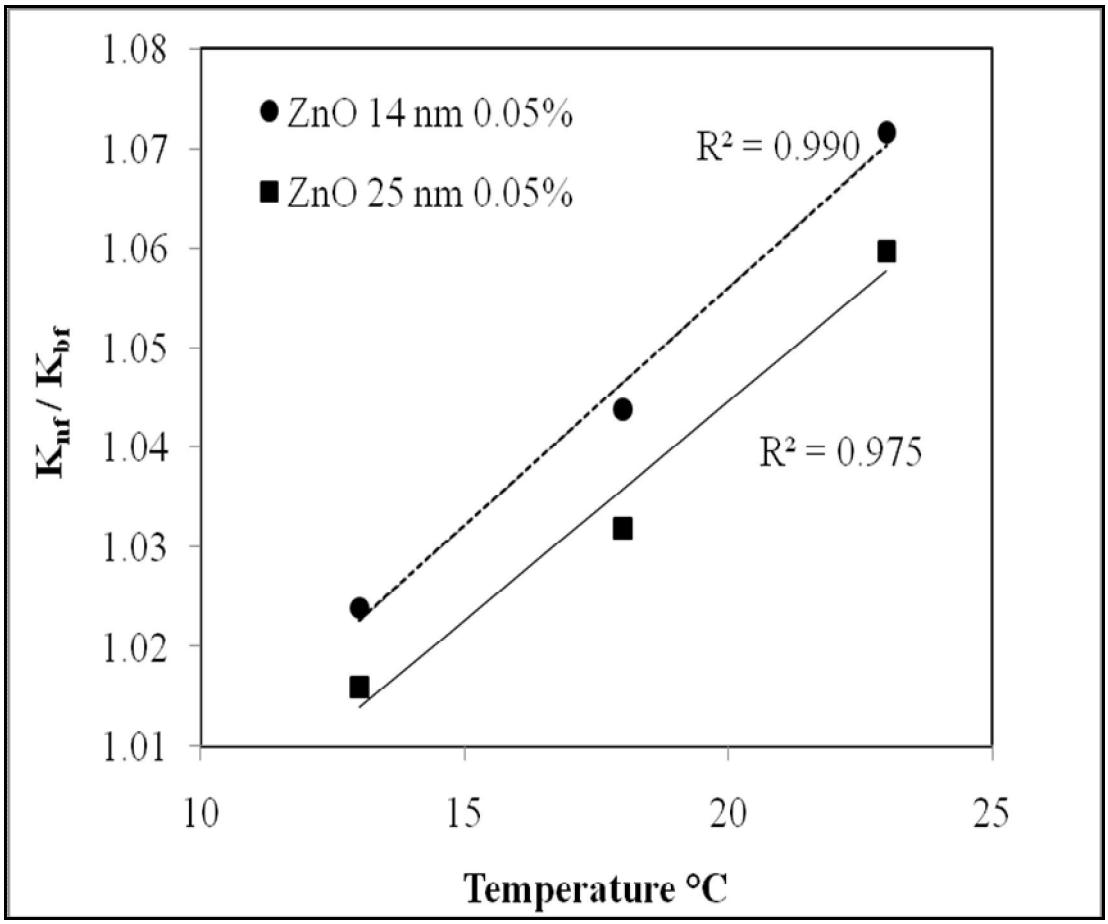

Figure 4.11: Thermal conductivity ratio variation with temperature for 14 nm and 25 nm diameter at 0.05% volume fraction.

In Figure 4.11, line 1: and line 2: show the variation of ZnO nanofluid of diameter 14 nm and 25 nm respectively at 0.05% volume fraction. The samples were prepared by dispersing ZnO nanoparticles into the basefluid (ethylene glycol) up to 4 hours. The relative thermal conductivity of ZnO based nanofluid increases, as the temperature increases.

Figure 4.12, shows the comparison of relative thermal conductivity of ZnO nanofluids with basefluids ethylene glycol and DI water at different volume fraction 0.01% and 0.05% with sonication time.

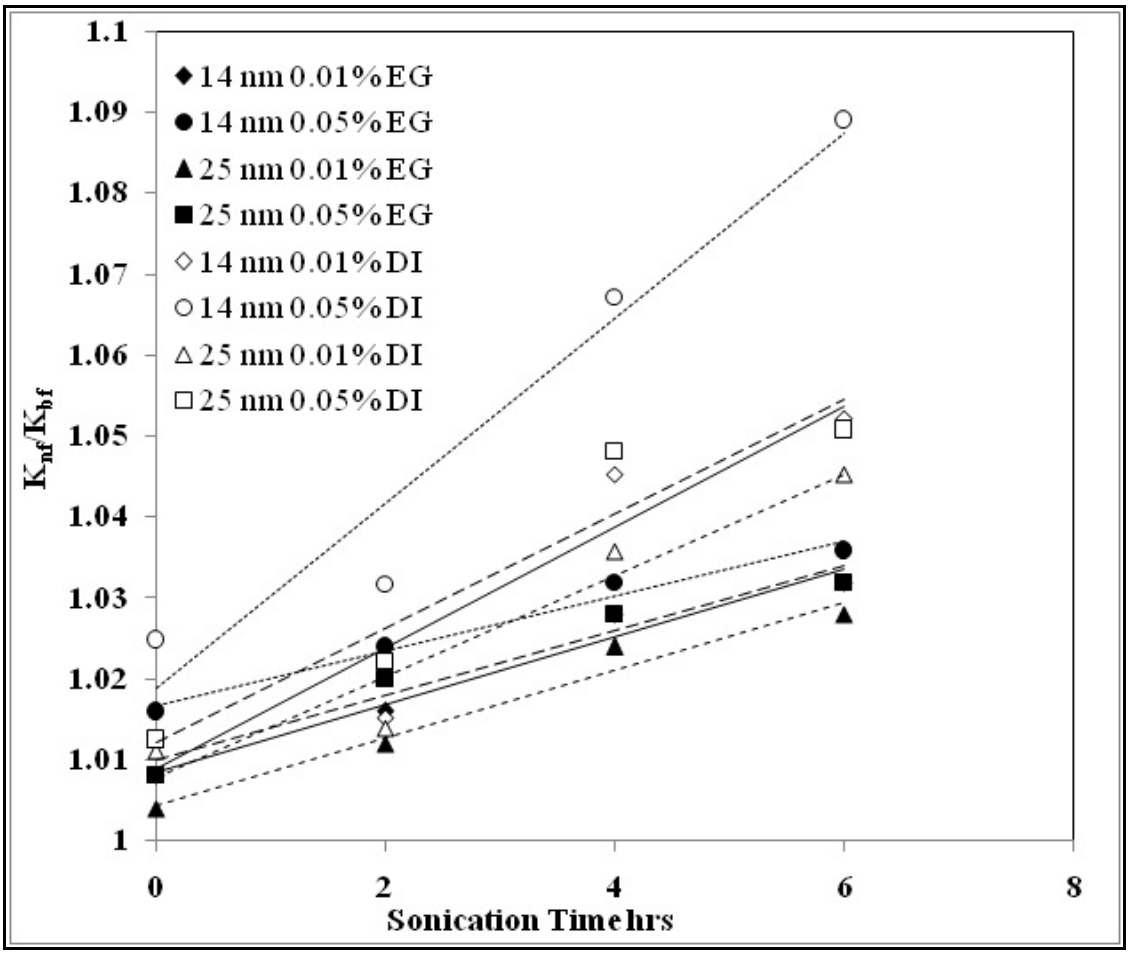

Figure 4.12: Comparison of relative thermal conductivity with basefluids Ethylene Glycol and DI water versus sonication time.

In Figure 4.12, the relative thermal conductivity of ZnO nanofluids increases for both basefluids ethylene glycol and DI water. The relative thermal conductivity of ZnO ethylene glycol based nanofluids show low enhancement as compared to DI water based nanofluids, because the ethylene glycol has more viscosity due to which ZnO nanoparticles takes more time to disperse in ethylene glycol basefluids. As a result, surface to volume ratio decreases in ethylene glycol based nanofluids. Therefore, the relative thermal conductivity of ZnO ethylene glycol based nanofluids show less increment as compare to DI water based nanofluids.

Figure 4.13, shows the comparison of relative thermal conductivity of ZnO nanofluids with basefluids ethylene glycol and DI water at different volume fraction 0.01% and 0.05% versus settling time.

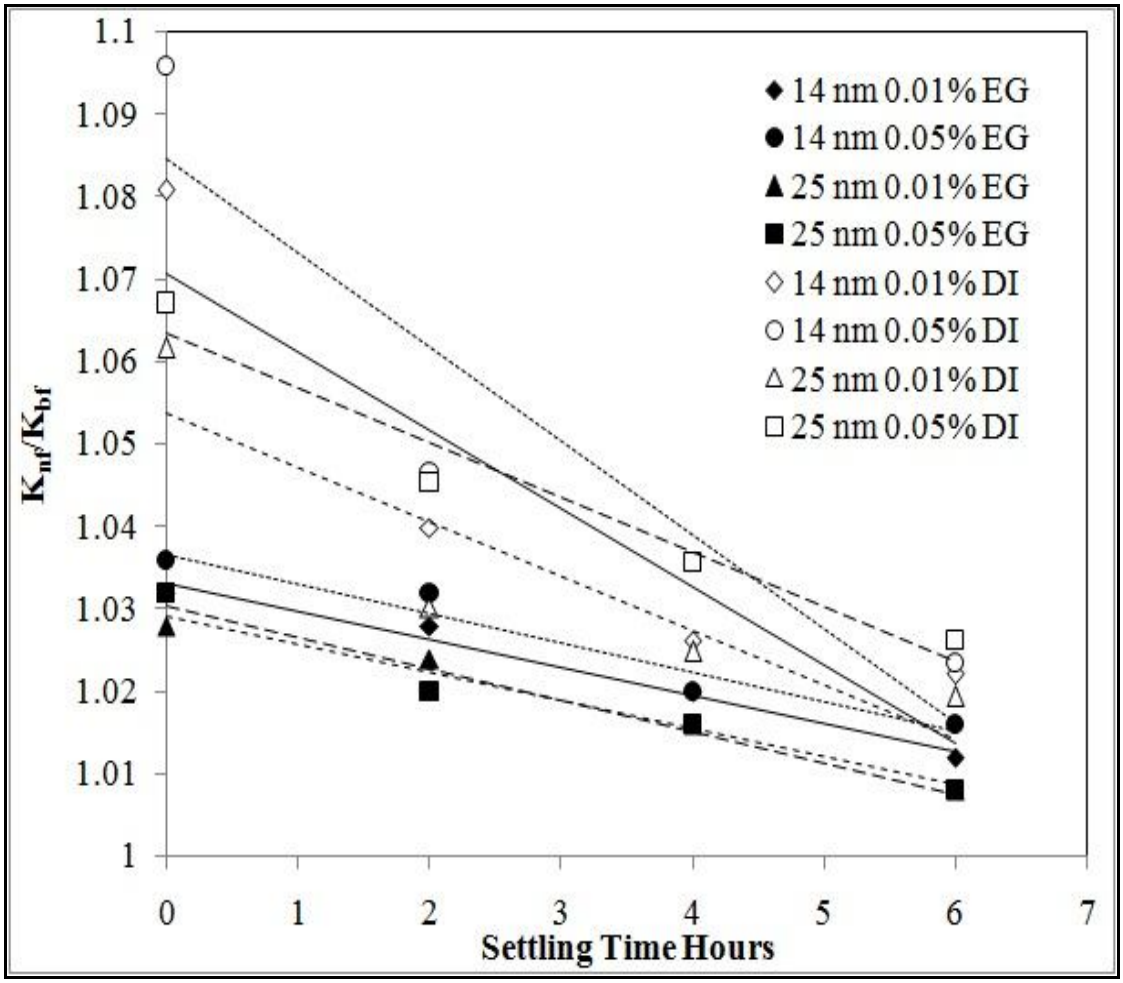

Figure 4.13: Comparison of relative thermal conductivity with basefluids Ethylene Glycol and DI water versus settling time.

The samples were prepared by dispersing nanoparticles in ultra bath sonicator up to 8 hours with basefluids ethylene glycol and DI water. The relative thermal conductivity of ZnO ethylene glycol and DI water based nanofluids decreases as the settling time increases because, as time increases the nanoparticles, which were dispersed in basefluids, starts agglomerated due to which

cluster formation visualize and settle down as the time increases. The decreases rate of relative thermal conductivity in ethylene glycol based nanofluids is less as compare to DI water based nanofluids because, the viscosity of ethylene glycol is more due to which nanoparticles will not settle down, as in DI water based nanofluids.

Figure 4.14, shows the comparison of relative thermal conductivity of ZnO nanofluids with basefluids ethylene glycol and DI water at volume fraction 0.05% versus settling time.

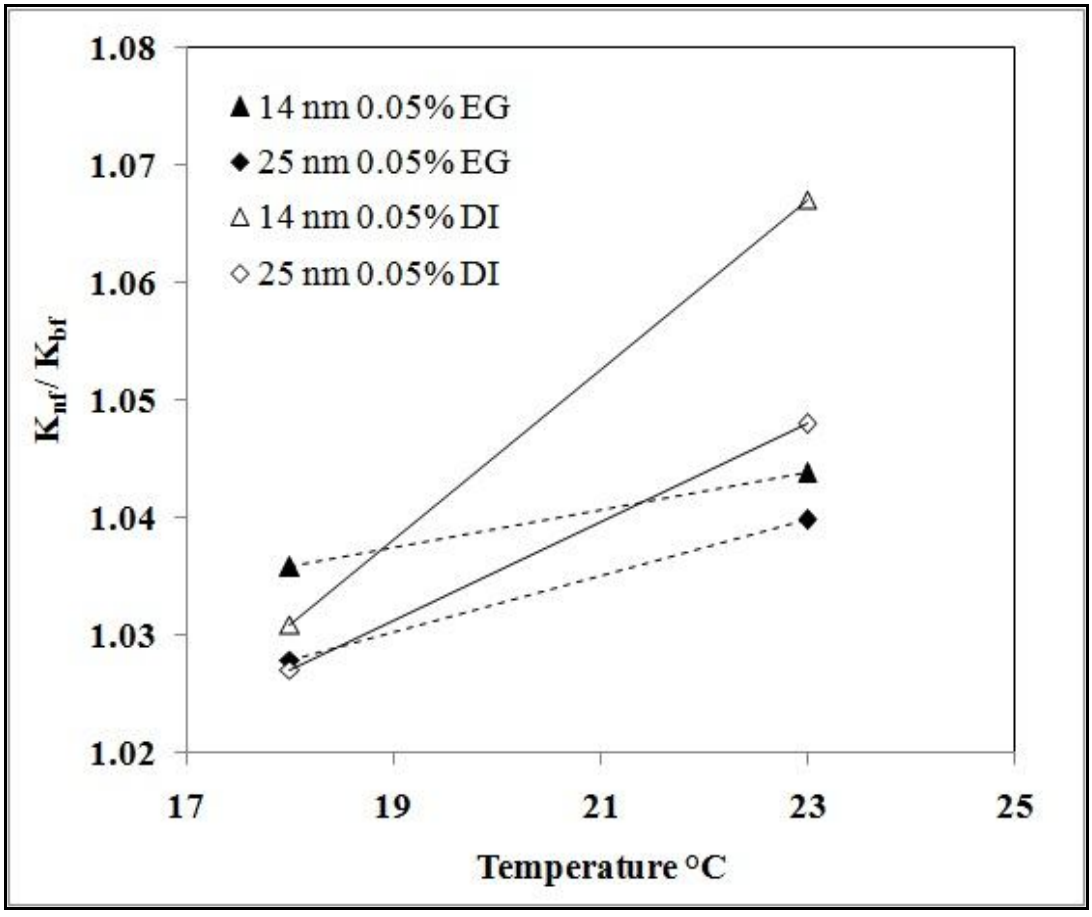

Figure 4.14: Comparison of relative thermal conductivity with basefluids Ethylene Glycol and DI water versus temperature

The samples were sonicated up to 4 hours with ethylene glycol and DI water based nanofluids. The relative thermal conductivity of ZnO ethylene glycol and DI water based nanofluids

increases as the temperature increases because, as the temperature increases Brownian motion of nanoparticles increase which excited the particles due to which random motion of nanoparticles increases and the particles starts strike with each other and transfer the heat energy. The increase rate of relative thermal conductivity in DI water based nanofluids is more as compare to ethylene glycol based nanofluids because, the viscosity of water is less as compare to ethylene glycol, due to which Brownian motion of nanoparticles is more in DI water based nanofluids. The trend for these data points is straight line and resulted best fit with R^2 value show in Figure 4.14.

Figure 4.15 shows the relative thermal conductivity of CNT nanofluids with basefluids DI water at different sonication power (140 – 220 W) of volume fraction 1% with sonication time.

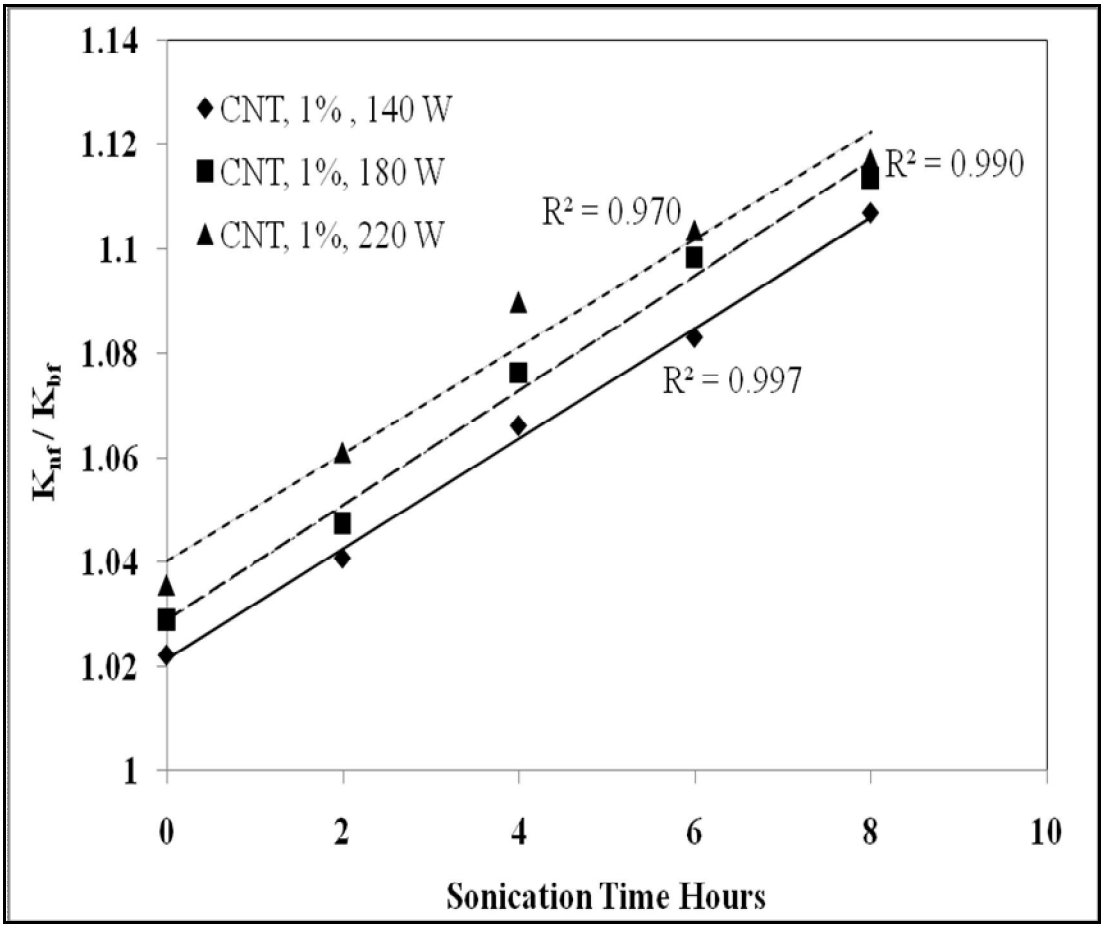

Figure 4.15: Thermal conductivity ratio variation with sonication time at different sonication power and volume fraction 1%.

In Figure 4.15, the relative thermal conductivity of CNT nanofluid rise as the sonication time increases. As the sonication power rise thermal conductivity increases because, as the sonication power increases the intensity of ultrasonic wave rise, which increases the suspension of nanoparticles in basefluid because, the agglomerated particles get break down due to which surface to volume ratio increases.

Figure 4.16, shows the relative thermal conductivity of CNT nanofluids with basefluids DI water at different sonication power (140 – 220 W) of volume fraction 1% with settling time.

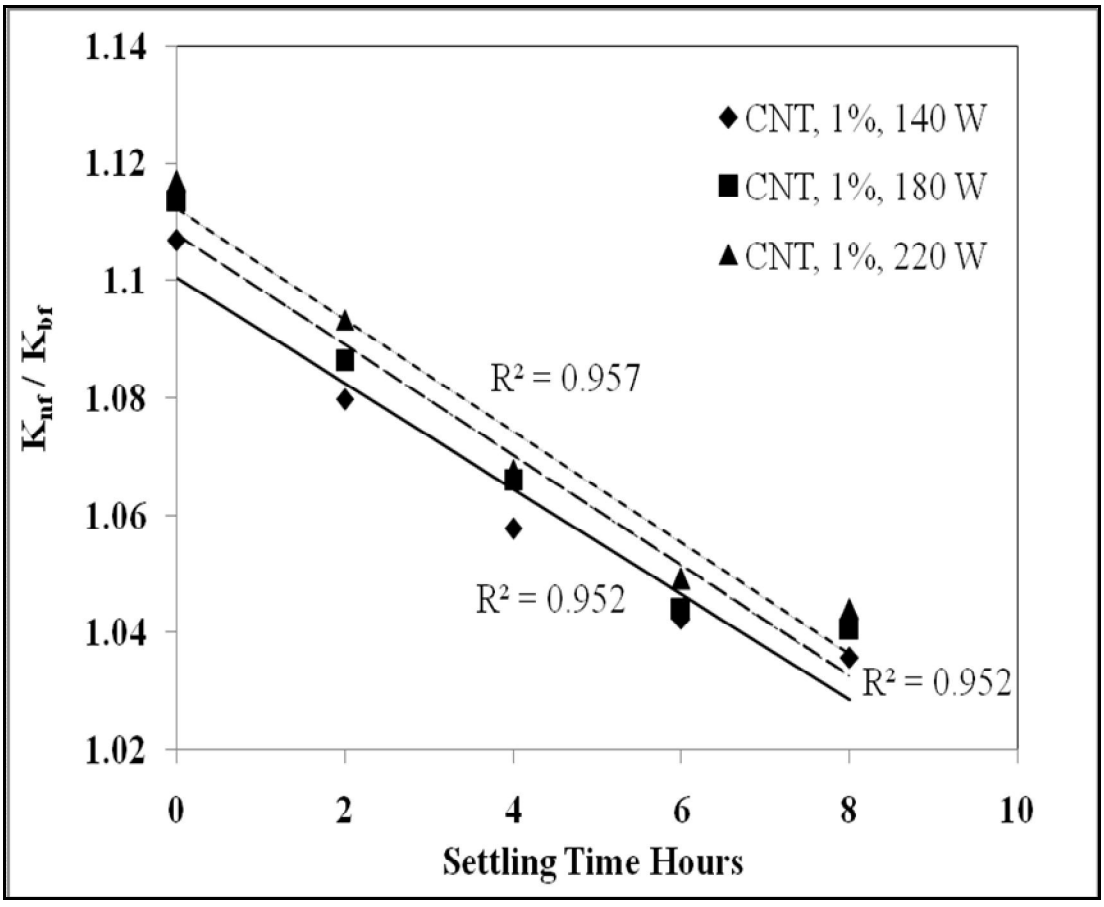

Figure 4.16: Thermal conductivity ratio variation with settling time at different sonication power and volume fraction 1%.

The samples were prepared by dispersing nanoparticles in probe ultra sonicator up to 8 hours. The thermal conductivity ratio of CNT nanofluid decreases as the settling time increases because, as the time increases the nanoparticles which were dispersed in basefluid, starts agglomerated due to which cluster formed and settle down as the time increases.

Figure 4.17, shows the relative thermal conductivity of CNT nanofluids with basefluids DI water at different sonication power (140 – 220 W) of volume fraction 1% with temperature

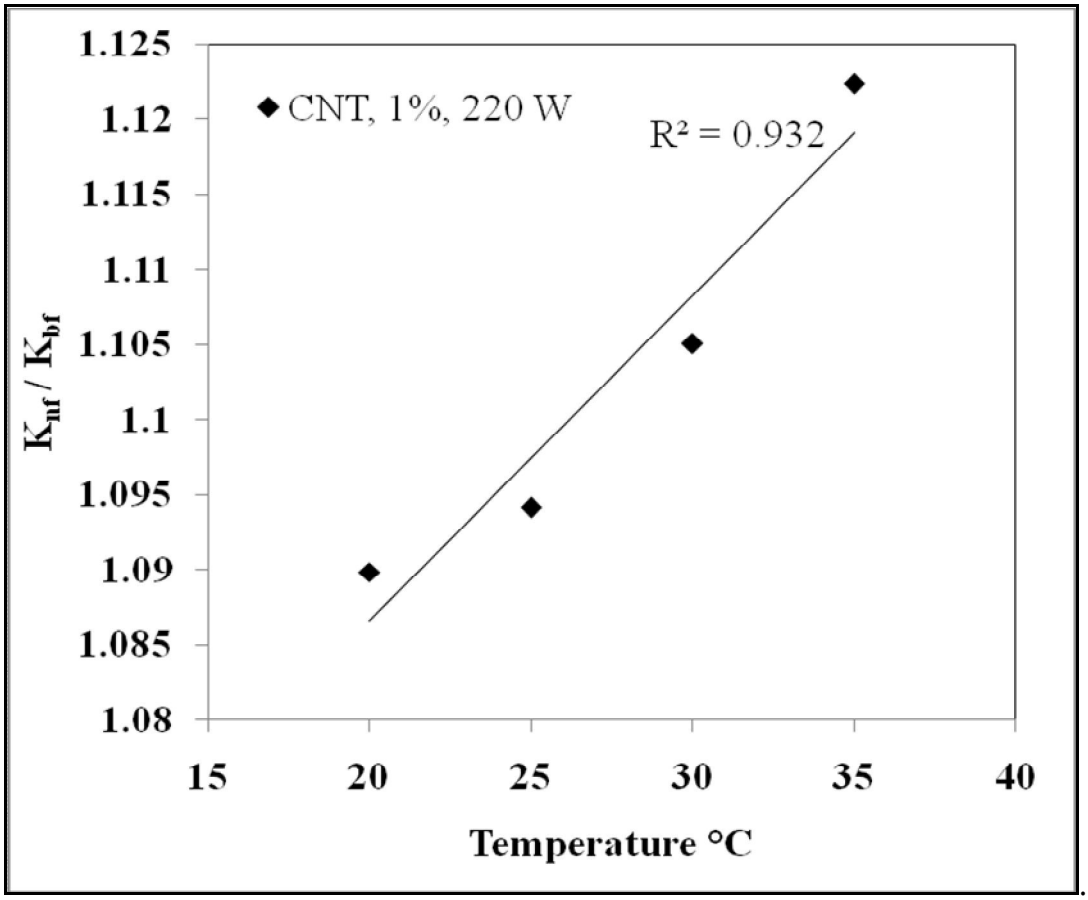

Figure 4.17: Thermal conductivity ratio variation with temperature at sonication power 220 W and volume fraction 1%.

The samples were prepared by 4 hours sonication in probe ultra sonicator. The relative thermal conductivity of CNT nanofluids increases as the temperature increases because, Brownian motion of nanoparticles increases due to which nanoparticles strike each other and transfer energy.

Figure 4.18, shows the relative thermal conductivity of aqueous silver nanofluids with basefluids DI water of volume fraction 4% with sonication time.

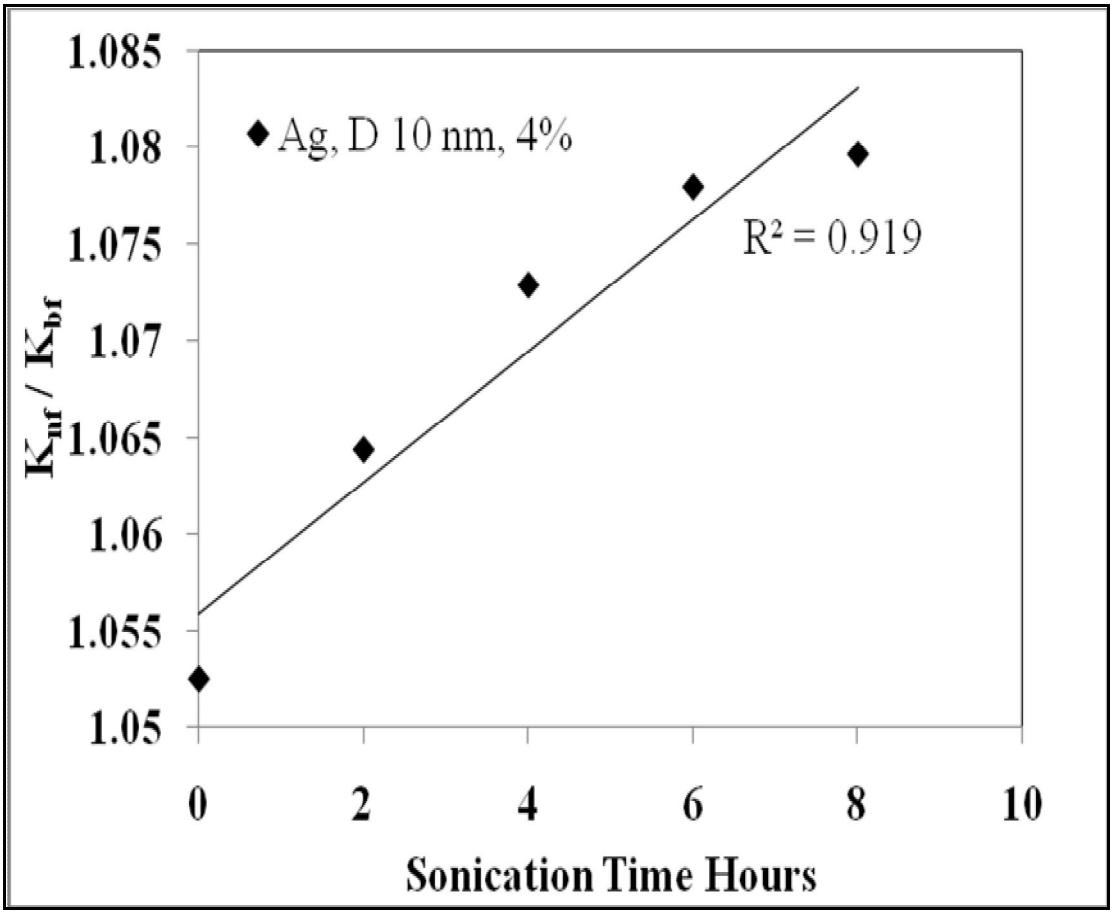

Figure 4.18: Thermal conductivity ratio variation with sonication time at volume fraction 4%.

The samples were sonicated from 0 to 8 hours to check the effect of sonication time on the relative thermal conductivity. The rate of enhancement in relative thermal conductivity is low

after 4 hours sonication time which shows, the relative thermal conductivity of aqueous silver nanofluids not get affected upon sonication time.

Figure 4.19, shows the relative thermal conductivity of aqueous silver nanofluids with basefluids DI water of volume fraction 4% with settling time.

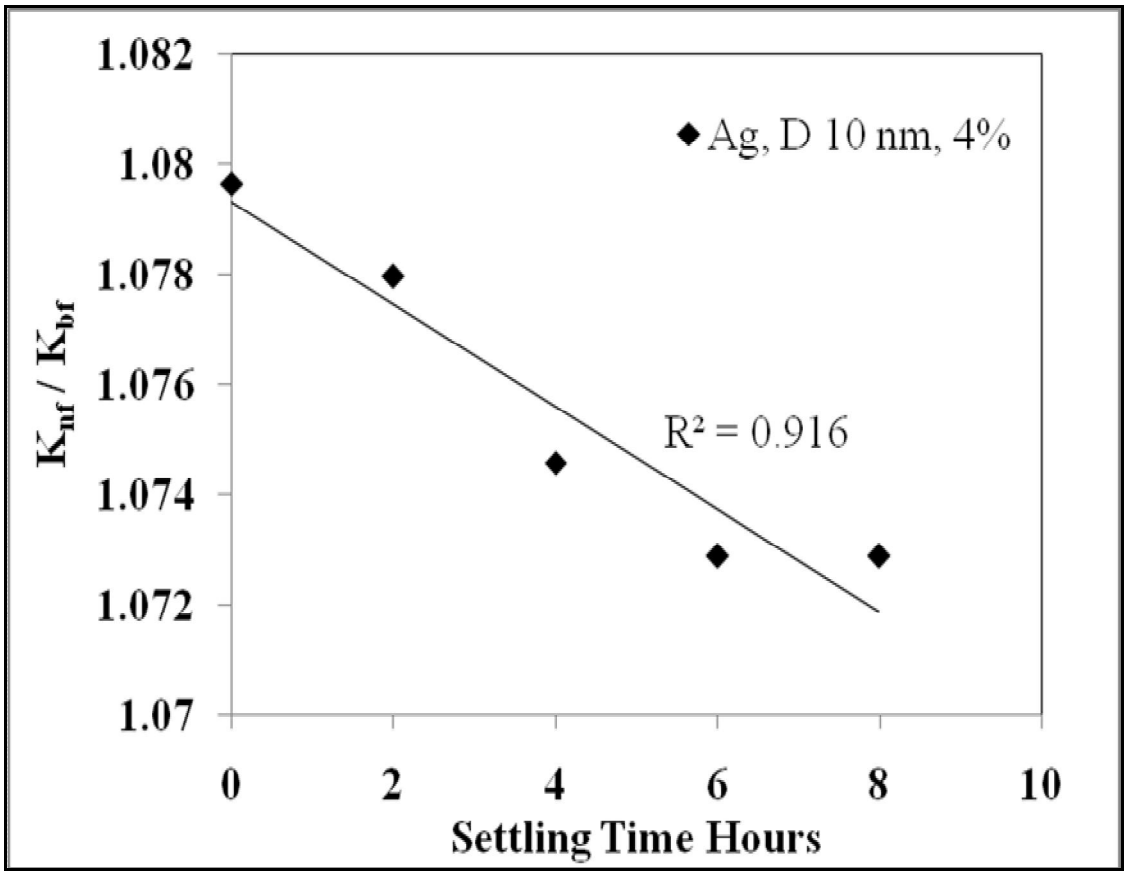

Figure 4.19: Thermal conductivity ratio variation with settling time at volume fraction 4%.

The rate of decrement in relative thermal conductivity is low because, aqueous silver nanoparticles were well dispersed in basefluid DI water. The settlement of nanoparticles after 6 hours was very low due to which relative thermal conductivity not decreases spontaneously.

Figure 4.20, shows the relative thermal conductivity of aqueous silver nanofluids with basefluids DI water of volume fraction 4% with temperature.

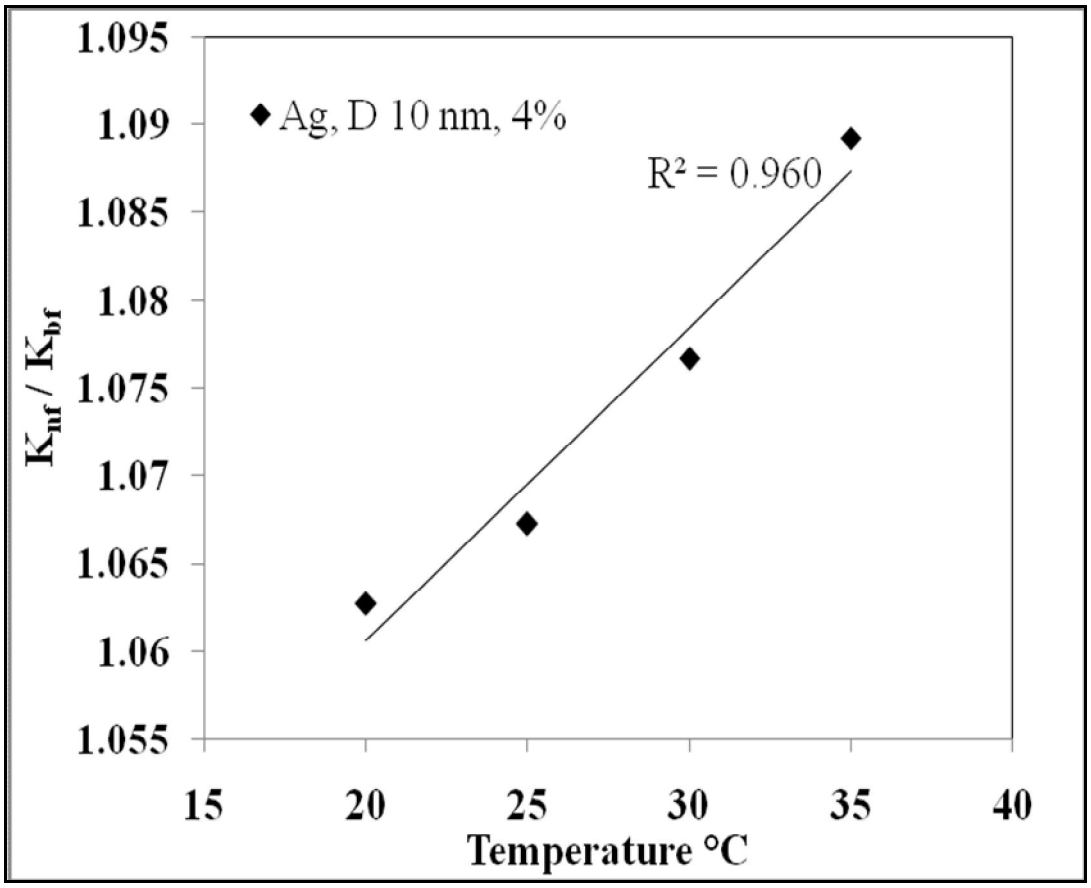

Figure 4.20: Thermal conductivity ratio variation with temperature at volume fraction 4%.

The samples were sonicated up to 4 hours sonication time. The relative thermal conductivity of aqueous silver nanofluids increases as the temperature increases because, as the temperature increases Brownian motion of nanoparticles increases which increases the collision of particles and transfer the heat energy.

CHAPTER 5: Development of new models for thermal conductivity of nanofluids

5.1 Theoretical modeling:

In particle-fluid mixtures, the nanoparticles are entirely covered by liquid molecules and form solid layered structure and the thickness of fluid layered over the particle is in nanometer (Jang et al. 2004). The nanoparticles assumed to be fully suspended in basefluid as shown in Figure 5.1,

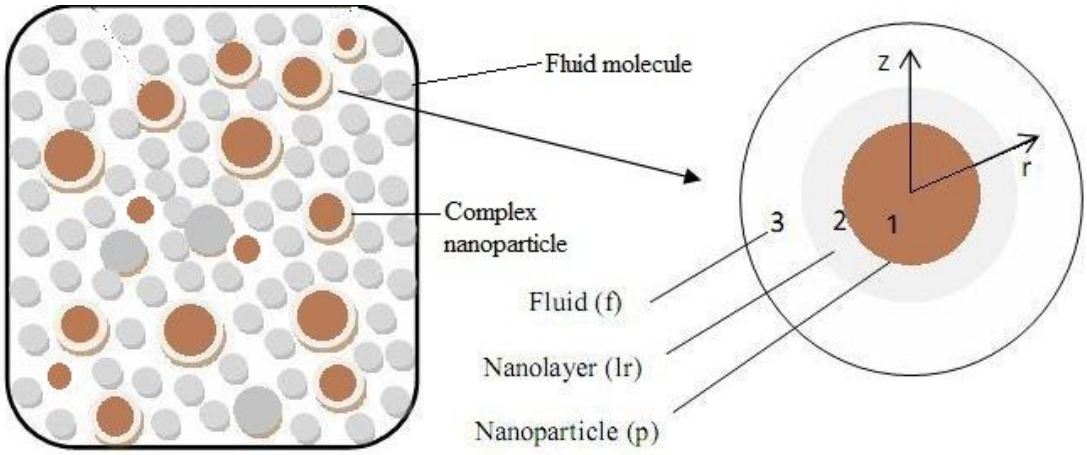

Figure 5.1: Schematic view of nanoparticles suspended in basefluid

Even though the random motion of nanoparticles is zero when time averaged, the vigorous and continously interactions between liquid molecules and nanoparticles at the molecular and nanoscale level translate into conduction at the macroscopic level, because there is no bulk flow (Jang et al. 2004). Brownian motion of nanoparticles in nanofluids produces convection like effects at the nanoscale (Jang et al. 2004). Therefore, heat flux $Q_{conduction}$ is equal to $Q_{convection}$ at micro scale level for a single particle

$$Q_{conduction} = K_p \frac{dt}{dr}$$

And

$$Q_{convection} = h \ \Delta T$$

$$K_p \times \frac{dt}{dr} = \frac{Nu \times K_{nf}}{d} \times \Delta T$$

Where Nu ~ Re^2 Pr^2 (Jang et al. 2004)

$$\mathrm{Re} = \frac{\rho \times V \times d}{\mu}$$

'V' is particle random motion, d is diameter of nanoparticles and μ is dynamic viscosity, velocity V is the ratio of nanoparticle diffusion coefficient to mean free path of basefluid molecule (Kumar et al., 2004)

$V = Do / L_f$

Where $Do = (K_b T) / (3 \Pi \mu d)$ (Einstein 1956)

Boltzman constant, $K_b = 1.38 \times 10{-}23$ J/K

$\mu = A \times 10^{B/(T-C)}$

$A = 2.414 \times 10^{-5}$, $B = 247.8$ and $C = 140$

Shams et al. (2012) gives equation 5.1

$$\frac{dt}{dr} = \frac{3 \times K_{lr}}{(K_p + 2 \times K_{lr})} \times T_\infty \qquad (5.1)$$

And Murshed et al. (2008) gives $K_{lr} = 3 \times K_{bf}$

Therefore, thermal conductivity for single nanoparticles in basefluid is (Re^2 Pr^2 = 'J' constant) equation 5.2

$$K_{nf} = \frac{3 \times K_{lr}}{(K_p + 2 \times K_{lr})} \times \frac{K_p}{\Delta T} \times \frac{d}{J} \qquad (5.2)$$

An attempt has been made for the fundamental modeling of thermal conductivity of nanofluids. The obtained equation 5.2 is made for single nanoparticle suspended in the basefluid. According to the literature survey of thermal conductivity of nanofluids done (Sham et al. 2012; Kumar et al. 2004 and Einstein 1956), some factors considered in the fundamental modeling of thermal conductivity of nanofluids which were not considered any researchers. Thus these factors further may be considered to calculate the thermal conductivity of nanofluids for the total volume fraction of nanoparticles in basefluids.

5.2 Development of empirical model for thermal conductivity based upon ZnO nanofluids

Mallick et al. (2013) gave the following model equation 5.3, to calculate the thermal conductivity of Al_2O_3 water and TiO_2 which was based upon Prandtl number and a new dimensionless quantity, which is ratio of Reynolds and Brinkman number for particle and fluids.

$$\frac{K_{nf}}{K_f} = Z\phi^{a}\ \mathrm{Pr}_p^{\ b}\ \mathrm{Pr}_f^{\ c}\left(\frac{\mathrm{Re}_p}{\sqrt{N_{BRp}}}\right)^{h} \tag{5.3}$$

The following model derived using regression analysis and the model given in equation 5.4 is obtained by using experimental data of ZnO-water nanofluids and ZnO-ethylene glycol nanofluids for a wide range of temperature, volume fraction and particle size.

$$\frac{K_{nf}}{K_f} = 1.0903\phi^{0.005}\ \mathrm{Pr}_p^{-0.006}\ \mathrm{Pr}_f^{-0.002}\left(\frac{\mathrm{Re}_p}{\sqrt{N_{BRp}}}\right)^{-0.003} \tag{5.4}$$

5.3 Evaluation of new developed model

To evaluate the accuracy of new developed model (equation 5.4) has been used to predict the thermal conductivity ratio for a wide range of data (volume fraction, temperature, particle size etc) and compare the thermal conductivity ratio of predicted versus experimental values.

In Figure 5.2, predicted values of thermal conductivity ratio obtained from new developed model (equation 5.4) compared with experimental values of thermal conductivity ratio obtained from Yu et al. (2009) of ZnO nanoparticles of diameter 15 nm, 5% volume fraction and for a same range of temperature.

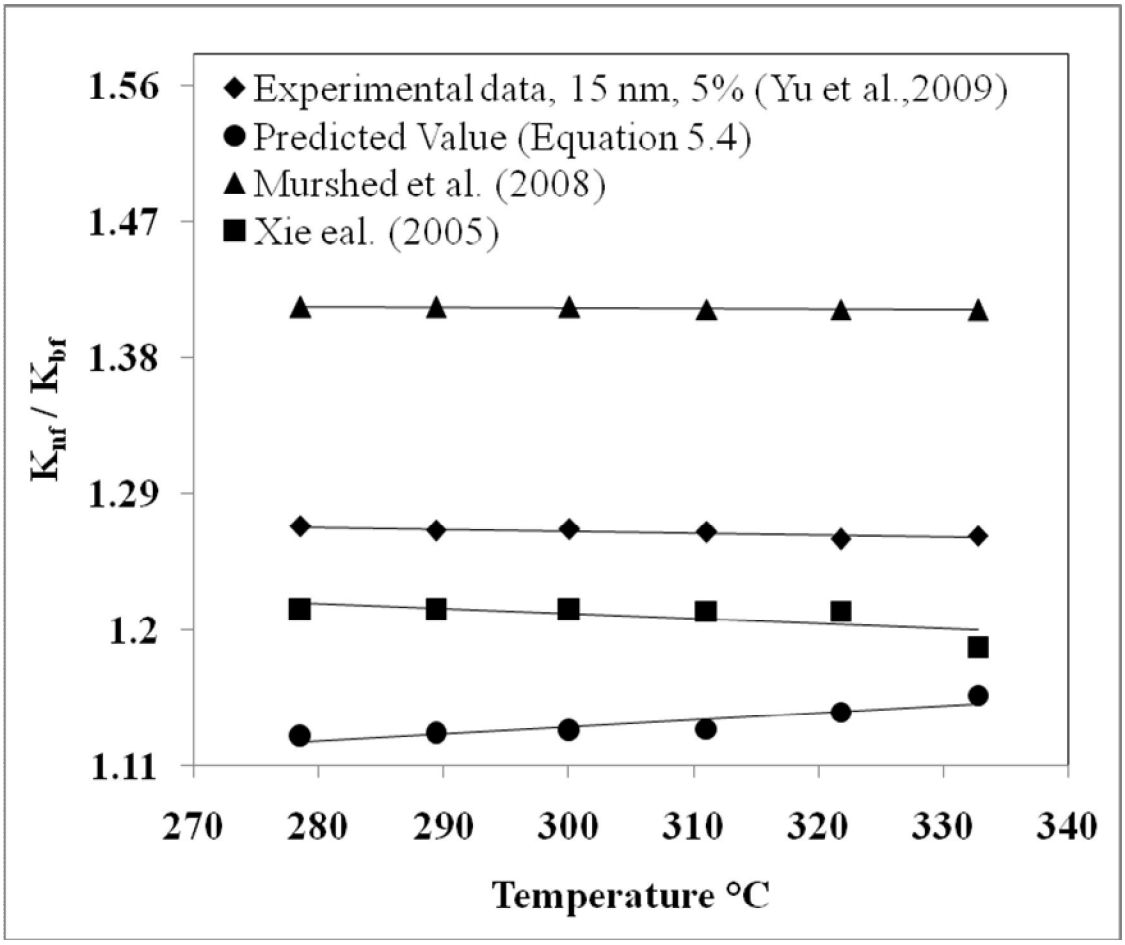

Figure 5.2: Predicted versus experimental values of thermal conductivity ratio with increase in temperature, D 15 nm, □ 5%

Figure 5.2 shows the values of thermal conductivity ratio obtained from new developed model (equation 5.4) which is under predicted the experimental values. The predicted values slightly converge to experimental values of thermal conductivity ratio as the temperature increases. The thermal conductivity ratio of Murshed et al. (2008) over predicted to experimental value. In Figure 5.3, predicted values of thermal conductivity ratio obtained from new developed model (equation 5.4) compared with experimental values of thermal conductivity ratio obtained from Yu et al. (2009) of ZnO nanoparticles of diameter 15 nm, temperature 30°C and for given volume fraction range.

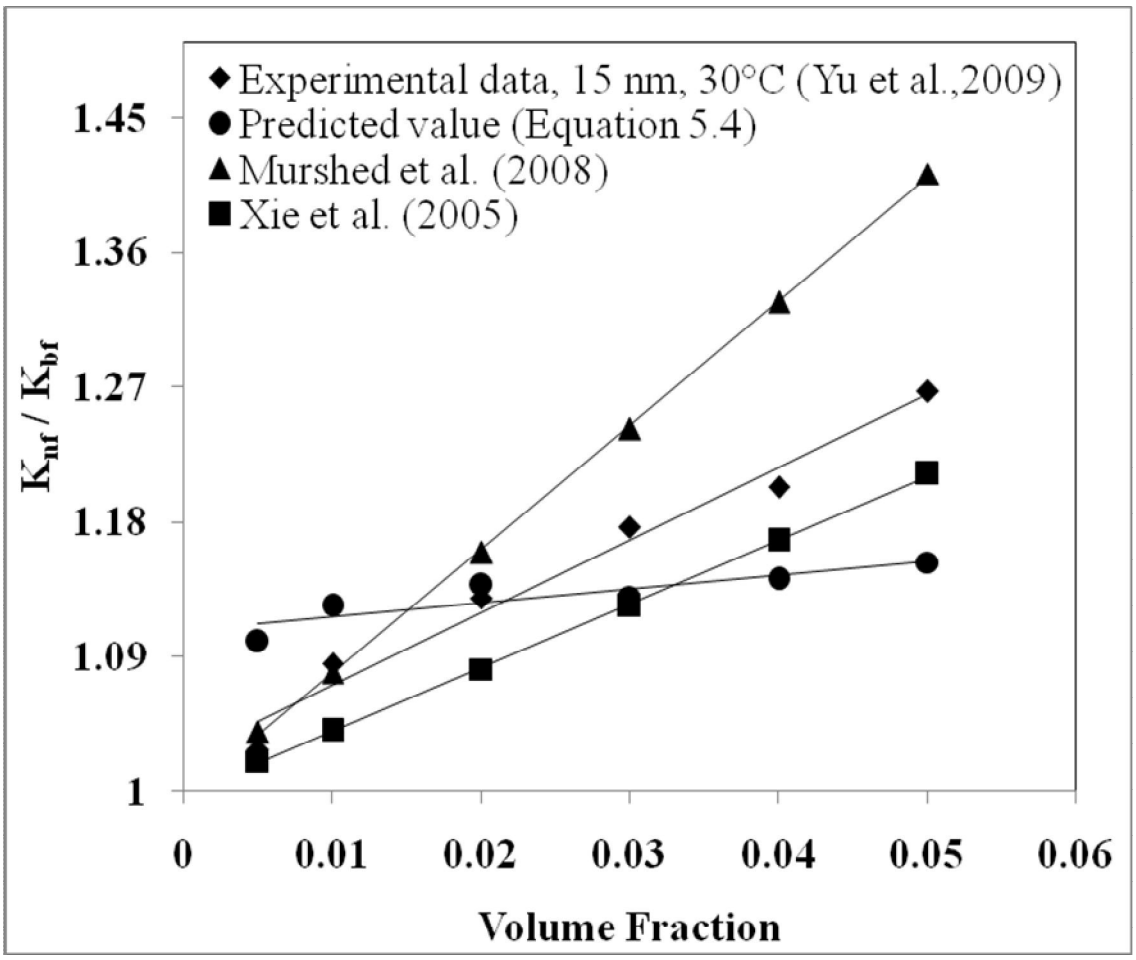

Figure 5.3: Predicted versus experimental values of thermal conductivity ratio with increase volume fraction, D 15 nm, T: 303 K

Figure 5.3 shows that the thermal conductivity ratio obtained from new developed model under predicted from volume fraction 0.005 to 0.02 and as the volume fraction increases from 0.02, the thermal conductivity of new developed model show more values compare to experimental values. In Figure 5.4, predicted values of thermal conductivity ratio obtained from new developed model (equation 5.4) compared with experimental values of thermal conductivity ratio obtained from Das et al. (2009) of ZnO nanoparticles of diameter 29 nm, 1% volume fraction and a given range of temperature.

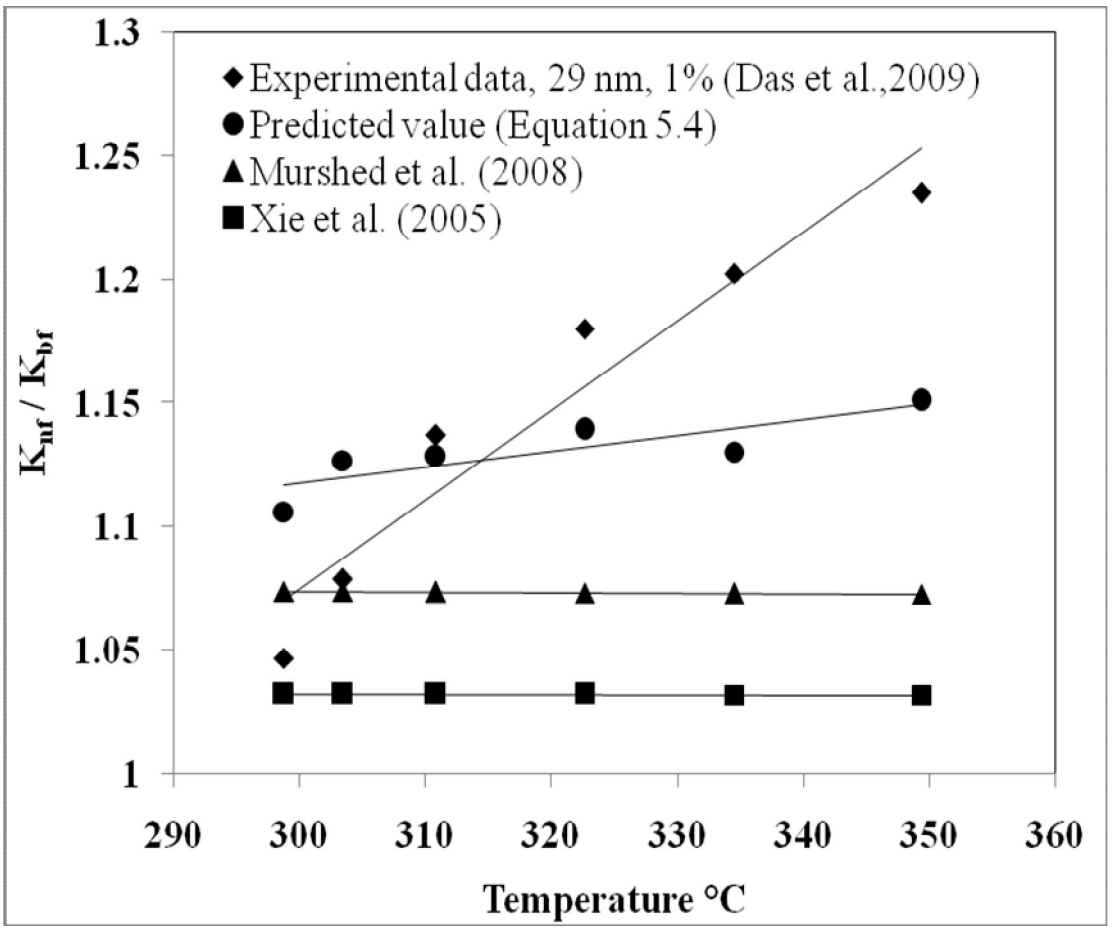

Figure 5.4: Predicted versus experimental values of thermal conductivity ratio with increase in temperature, D 29 nm, □ 1%.

Figure 5.4, shows that the thermal conductivity ratio obtained from new developed model over predicted (293-312 K) and under predicted after temperature increase from 312 K. As the temperature increases, the predicted and experimental thermal conductivity ratio also increases. The thermal conductivity ratio of Murshed et al. (2008) and Xie et al. (2005) under predicted to experimental values. In Figure 5.5, predicted values of thermal conductivity ratio obtained from new developed model (equation 5.4) compared with experimental values of thermal conductivity ratio obtained from Das et al. (2009) of ZnO nanoparticles of diameter 77 nm, 4% volume fraction and a given range of temperature.

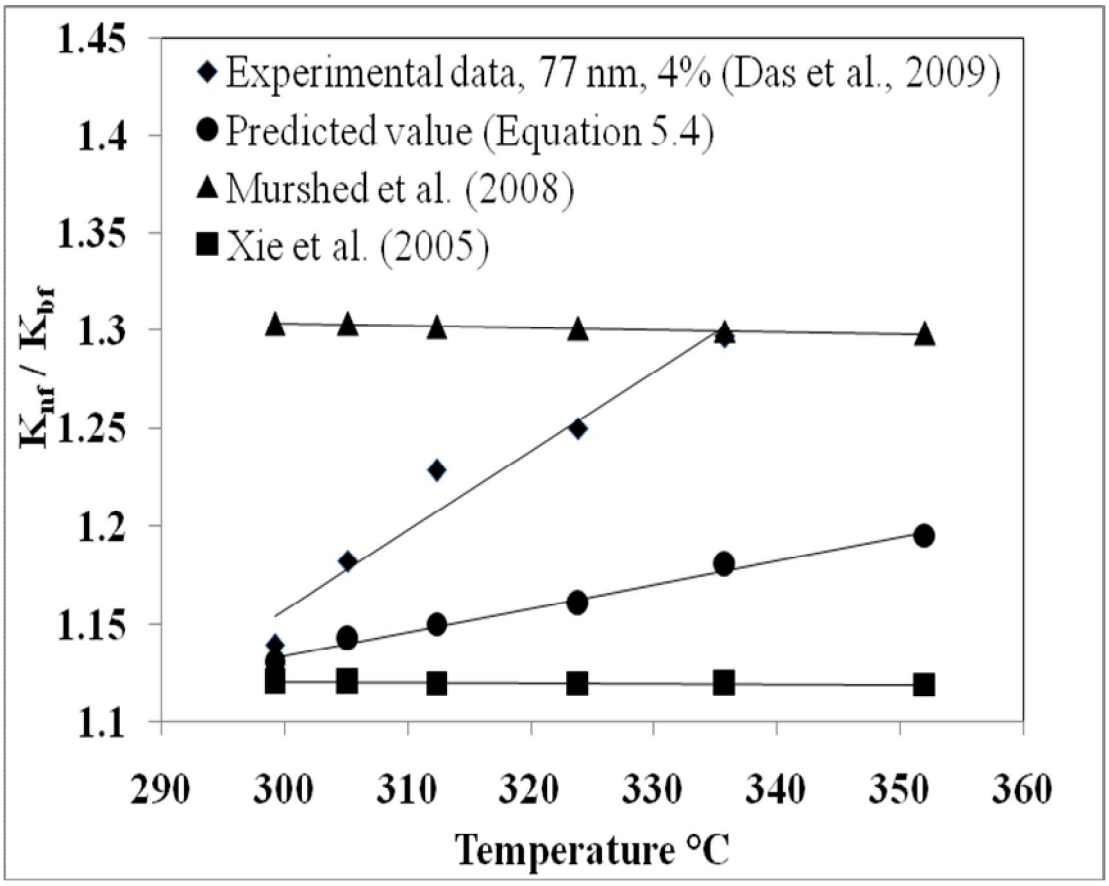

Figure 5.5: Predicted versus experimental values of thermal conductivity ratio with increase in temperature, D 77 nm.

Figure 5.5 shows that at volume fraction 4%, as the temperature increases the predicted thermal conductivity ratio also increases but under predicted experimental values. As the temperature increases, the predicted thermal conductivity ratio starts diverging from experimental values.

To indicate the predication accuracies of the new developed model (equation 5.4), Table 5.1 shows the average of sum of absolute values of relative error for thermal conductivity ratio using the formula given below.

$$\text{Relative error} = \sum_{n} \left| \frac{\text{experimental value - predicted value}}{\text{experimental value}} \right| \times 100\%$$

Table 5.1: Relative Errors of New Developed Model Predictions (%)

Figures	**New developed model for ZnO (Equation 5.4)**
5.2	9.09
5.3	1.08
5.4	1.15
5.5	6.73

From the above relative error analysis, it is observed that the new developed model shows inaccuracy range 1.08-9.93% and shows good agreement for low volume fraction up to 2% and at low temperature as compared to Murshed et al. (2008), Xie et al. (2005), Yu and choi (2003), Mintsa et al. (2009) and Peterson et al. (2006) models as shown in chapter 2 and table 2. . As the temperature and volume fraction increases, new developed model not show good agreement in predicted and experimental thermal conductivity ratio values.

Chapter 6: Conclusion and Future Scope of Work

6.1 Conclusion

a) The existed theoretical and empirical models have been evaluated, to predict the thermal conductivity of nanofluids for a wide range of experimental conditions and compared with available experimental values of CuO-water nanofluids and the results revealed that the existing models show error within 0.17 - 49.31 % range.

b) Enhancement in thermal conductivity of ZnO and single wall carbon nanotubes DI water based nanofluids as the sonication time, volume fraction and temperature increases and there is less increment in aqueous silver DI water based nanofluids.

c) The thermal conductivity of ZnO ethylene glycol based nanofluids, show less increment as compare to ZnO DI water based nanofluids.

d) As the settling time and size of nanoparticles increases the thermal conductivity of all the nanofluids decreases. In single wall carbon nanotubes based nanofluids, as the sonication power increases the thermal conductivity of nanofluids increases.

e) A new empirical model has been developed to calculate the thermal conductivity ratio of ZnO based nanofluids using regression analysis. The predicted thermal conductivity ratio of new developed model shows good agreement with experimental values at low volume fraction and as the temperature increases, the error between predicted and experimental thermal conductivity ratio increases.

f) A theoretical model has been made to calculate thermal conductivity of nanofluids for a single nanoparticle.

6.2 Future Scope of Work

a) Develop theoretical model to calculate the thermal conductivity of nanofluids for different nanoparticles by considering different parameters such as clustering effect, pH, interfacial layer, brownian motion and surfactant uses.

b) Design a standard instrument to measure the thermal conductivity of nanofluids. Measurement of thermal conductivity of nanofluids is also issue because, the reading obtained from KD2 Pro is irreproducible.

c) More work has been carried out to stable nanoparticles in the basefluids.

Appendix

Appendix A

Figure 4 A1: Magnetic stirrer with hot plate

Figure 4 A2: Ultra probe sonicator

Figure 4 A3: Experimental setup

List of symbols

K_f : Thermal conductivity of basefluid (W/mK)

K_p : Thermal conductivity of nanoparticles (W/mK)

K_{nf} : Thermal conductivity of nanofluid (W/mK)

K_{lr} : Thermal conductivity of interfacial layer (W/mK)

t : Bulk temperature of nanofluid (^{0}C)

f : fluids

lr : nanolayer (nm)

r : radius of nanoparticles (nm)

$Q_{conduction}$: heat flux in conduction (w/m^2)

$Q_{convection}$: heat flux in convection (w/m^2)

h : heat transfer coefficient (w/m^2k)

Nu : Nusselt number $(h \times d) / K_{nf}$

Re : Reynold number $(\rho \times V \times d) / \mu$

Pr : Prandtl number $(\mu \times C_p) / K_p$

C_p : specific heat (Kj / Kg K)

ρ : density of basefluid (Kg / m^3)

V : particle random motion (m / s)

μ : dynamic viscosity of basefluid (Kg / m s)

D_o : nanoparticle diffusion coefficient

L : mean free path of basefluid molecule

T : temperature (K)

K_b : boltzman constant ($1.38 \times 10\text{-}^{23}$ J / K)

Greek symbols

φ : Volume fraction of nanoparticles in nanofluids

α : Ratio of thermal conductivity of particle to that of base fluid

γ : Ratio of nanolayer thickness to radius of nanoparticles

δ : Nanolayer (interfacial) thickness

Abbreviation

EG : Ethylene glycol

DI : Deionized Water

Subscripts

nf : nanofluid

p : nanoparticle

bf : basefluid

lr : interfacial layer (nm)

References

Ashly S., 1994, Small-scale Structure Yields Big Property Payoffsfl, Mechanical Engineering, Vol. 116, Issue. 2, PP. 52-57.

Beck Michael P., Yuan Yanhui, Warrier Pramod and Teja Amyn S., 2009, The effect of particle size on the thermal conductivity of alumina nanofluids, J Nanopart Res (2009) 11:1129–1136

Bruggeman D.A.G., 1935, Berechnung verschiedener physikalischer Konstanten von heterogenen Substanzen. I. Dielektrizitätskonstanten und Leitfähigkeiten der Mischkörper aus isotropen Substanzen, Annalen der Physik, Vol. 416, Issue 7, PP. 636–664.

Buhr E., Senftleben N,, Klein T., Bergmann D., Gnieser D., Frase C. G. and Bosse H., 2009,Characterization of nanoparticles by scanning electron microscopy in transmission mode, Measurement Science and Technology, Vol. 20, Issue. 084025, PP. 1-9

Calvin H. Li,, Peixue Jiang, and G. P. Peterson, 2013, Dual Role of Nanoparticles in the Thermal Conductivity Enhancement of Nanoparticle Suspensions, Journal of Nanofluids Vol. 2, pp. 20–24

Cullity B.D. and Stock S.R., 2001, Elements of X-Ray Diffraction, Third Edition, Pub. Prentice Hall.

Chopkar M., Sudarshan S., Das P.K., and Manna I., 2008, Effect of Particle Size on Thermal Conductivity of Nanofluid, Metals & Materials Society, Volume 39 A, PP. 1535-1542.

Das S.K., Putra N., Thiesen P. and Roetzel W., 2003, Temperature Dependence of Thermal Conductivity Enhancement for Nanofluids, Heat Transfer, Vol. 125, PP. 567-574.

Das S.K., Choi S.U.S., Yu W. and Pradeep K., 2008, Nanofluids Science and Technology, Publ. Wiley Interscience.

Das D.K. and Vajjha R.S., 2009, Experimental Determination of Thermal Conductivity of Three Nanofluids and Development of New Correlations, Heat and Mass Transfer, Vol. 52, PP. 4675–4682.

Eastman J. A., Choi U. S., Li S., Thompson L. J., and Lee S., 1997, Enhanced Thermal Conductivity through the Development of Nanofluids, Y Proc. of the Symposium on Nanophase and Nanocomposite Materials H, Materials Research Society, Boston, Vol. 457, PP. 3-11.

Einstein. A, 1956 Investigation on the Theory of Brownian Movement, Dover, New York.

Gabriel B.L., 1985, SEM: A User Manual For Material Science, American Society For Metals.

Gilles R., Cong T. M., and Mintsa H.A., 2007, New Temperature Dependent Thermal Conductivity Data of Water Based Nanofluids, Int. Conference on Heat Transfer, Thermal Engineering and Environment, Athens, Greece, August 25-27, 2007 290

Gleiter, H., 1989, Nanocrystalline Materials, Prog. Material Science, Vol. 33, PP. 223-315.

Granqvisq C. G., and Buhrrnan, R. A., 1976, Ultrtilne Metal Particles, J Applied Physics, vol.47, PP. 2200.

Hojjat M, Etemad S, Bagher R, Thibault J, 2011, Thermal conductivity of non Newtonian nanofluids: Experimental data and modeling using neural network, International Journal of Heat and Mass Transfer vol 54, PP. 1017–1023.

Jang S.P. and Choi S.U.S., 2004, Role of Brownian motion in the enhanced thermal conductivity of nanofluids, Appl. Phys. Lett., 84, pp. 4316-4318.

Kimoto K., Kamilaya Y., Nonoyama M., and Uyeda R., 1963, An Electron Microscope study on Fine Metal Particles Prepared by Evaporation in Argon Gas at Low Pressure, Jpn. J. Appi. Phys., Vol. 2, PP. 702.

Kestin jospeh, Sokolov Mordechia and Wakehalm William A., 1978, viscosity of liquid water in the range -8°C to 150°C, J. Phys. Chem.. Ref. Data, Vol. 7, No. 3.

Kondaraju Sasidhar, Jin E.K. and Lee Joon Sang, 2010, Direct numerical simulation of thermal conductivity of nanofluids: The effect of temperature two-way coupling and coagulation of particles, International Journal of Heat and Mass Transfer 53, 862–869

Koo J. and Kleinstreuer C., 2004, A New Thermal Conductivity Model for Nanofluids, Nanoparticle Research, Vol. 6, PP. 577–588.

Kumar D.H., Patel H.E., Kumar V.R.R., Sundararajan T., Pradeep T., and Das S.K., 2004, Model for Heat Conduction in Nanofluids, Phys. Rev. Lett., 93, 144301.

Kwak K. and Kim C., 2005, Viscosity and Thermal Conductivity of Copper Oxide nanofluid Dispersed In Ethylene Glycol, Korea-Australia Rheology , Vol. 17, Issue. 2, PP. 35-40.

Mallick S.S., Mishra A., and Kundan L, 2013, An investigation into modeling thermal conductivity for alumina-water nanofluids, Powder technology, pages234-244.

Mintsa H.A., Roy G., Nguyen C.T. and Doucet D., 2009, New Temperature Dependent Thermal Conductivity Data for Water Based Nanofluids, Thermal Sciences, Vol. 48, PP. 363–371.

Murshed S.M.S., Leong K.C. and Yang C., 2008, Investigations of Thermal Conductivity and Viscosity of Nanofluids, Thermal Sciences, Vol. 47, PP. 560–568.

Murshed S.M.S., Leong K.C. and Yang C., 2005, Enhanced thermal conductivity of TiO2—water based nanofluids, International Journal of Thermal Sciences, Vol. 44, PP. 367–373.

Namburu Praveen K., Kulkarni Devdatta P., Misra Debasmita and Das Debendra K., 2007, Viscosity of copper oxide nanoparticles dispersed in ethylene glycol and water mixture, Experimental Thermal and Fluid Science 32 397–402

Peterson G.P and Li C.H.., 2006, Experimental Investigation of Temperature and Volume Fraction Variations on The Effective Thermal Conductivity of Nanoparticle Suspensions (Nanofluids), Applied Physics, Vol. 99, Issue. 08314, PP. 1-8.

Suryanarayana C., Norton M.G., 1998, X-Ray Diffraction: A Practical Approach, Pub. Springer.

Waseda Y., Matsubara E. and Shinoda K., 2001,X-Ray Diffraction Crystallography, Pub. Springer.

Shah M.A.,and Ahmad Tokeer., 2010, Principles of nanoscience and nanotechnology, Publication Narosa.

Shams Z, Mansouri S. H. and Baghban M., 2012, A Proposed Model for Calculating Effective Thermal Conductivity of Nanofluids, Effect of Nanolayer and Non-Uniform Size of Nanoparticles, J. Basic. Appl. Sci. Res., 2(9)9370-9377.

Teng T.P., Hung Y.H., Teng T.C., Moa H.E. and Hsu H.G., 2010, The Effect of Alumina/Water Nanofluid Particle Size on Thermal Conductivity, Thermal Engineering, Vol. 30, PP. 2213-2218.

Wenhua Yu, David M. France, Elena V. Timofeeva, and Dileep Singh, 2013, Effective Thermal Conductivity Models for Carbon Nanotube-Based Nanofluids, Journal of Nanofluids Vol. 2, pp. 69–73

Wang X., Xu X. and Choi S.U.S., 1999, Thermal Conductivity of Nanoparticle- Fluid Mixture, Thermo Physics and Heat Transfer, Vol. 13, Issue. 40, PP. 474-480.

Wang Wei, Lin Lin, XiaoFeng Zhou and Wang Shengyue, 2012, A Comprehensive Model for the Enhanced Thermal Conductivity of Nanofluids, Journal of Advanced Research in Physics 3(2), 021209

Xie H., Fujii M. and Zhang X., 2005, Effect of Interfacial Nanolayer on The Effective Thermal Conductivity of Nanoparticle-Fluid Mixture, Heat and Mass Transfer, Vol. 48, PP. 2926–2932.

Yu W. and Choi S.U.S., 2003, The Role of Interfacial Layers in The Enhanced Thermal Conductivity of Nanofluids: A renovated Maxwell model, Nanoparticle Research, Vol. 5, PP. 167–171.

Yu W., Xie H., Chen L. and Li Y., 2009, Investigation of thermal conductivity and viscosity of ethylene glycol based ZnO nanofluid, Thermochimica Acta 491 (92–96).

Zhang X. and Fujii M., 2000, Simultaneous Measurements of The Thermal Conductivity and Thermal Diffusivity of Molten Salts with A Transient Short-Hot-Wire Method, Thermo physics. Vol. 21, Issue 1, PP. 71–84.

Zhu H.T., Zhang C.Y., Tang Y.M., and Wang J. X, 2007, Novel Synthesis and Thermal Conductivity of CuO Nanofluid, J. Phys. Chem. C, 111, 1646-1650

Zhu H., Han D., Meng Z., Wu D. and Zhang C., 2011, Preparation and thermal conductivity of CuO nanofluid via a wet chemical method, Nanoscale Research Letters, 6:181.